Chapter 12
Reflector Antennas

Michael E. Cooley and Daniel Davis

Electronic Systems
Northrop Grumman Corporation

12.1 INTRODUCTION

Role of the Radar Reflector Antenna. Radar reflector antennas provide the means by which the transmit (receive) energy and its associated waveform is radiated into (coupled from) free space. In transmit mode, the antenna launches a guided wave from the transmitter into free space and typically focuses this radiated energy over a limited angular range or beamwidth. In receive mode, the reflector antenna operates in a reciprocal manner, receiving reflected radar target energy, i.e., echoes, from a limited angular range. These received echoes are then converted into guided waves that are amplified and subsequently processed in the radar receiver.

Typically, the radar reflector antenna must be designed to enable beam scanning over the field-of-view (FOV) via either mechanical or electronic means (or some combination of both). In Section 12.4, methods of electronic beam scanning (limited FOV) using array feeds are discussed. Thus, the radar reflector antenna performs several important functions: (1) It converts the guided wave from the transmitter to a radiated wave (or vice versa on receive); (2) It concentrates or collimates the radiated energy into a directive beam of specified gain and beamwidth; (3) It collects the reflected energy scattered from the radar target; and (4) It supports beam scanning via either electronic or mechanical means (or both).

Antenna Beam Scanning. For most radar applications, the trade or choice between a reflector antenna and a direct radiating phased array is typically driven by factors relating to scan rate, scan volume, and cost. Reflector antennas are typically employed in a radar when (1) slower scan rates are sufficient and mechanical scanning suffices, and/or (2) a very high gain (electrically large) aperture is required and a phased array, i.e., an electronic scanning array (ESA), is cost prohibitive, and/or (3) the required scan volume is limited and can be satisfied via use of an array-fed reflector. During the 1980s and 1990s, phase shifter and T/R module technology greatly matured and ESA costs dropped dramatically. These advances have resulted in increased interest and utilization of ESAs for wide scan radar applications, and array-fed reflectors where limited electronic scan suffices.

Advantages and Applications of the Radar Reflector Antenna. In the previous paragraph, the proliferation of ESA antennas in modern radar systems is linked to the

dramatic T/R module cost reductions and technology improvements. The improved performance of ESA radars is cited as a reason for decreased utilization of reflector antennas in many of today's radar system designs.

However, there are still applications where the reflector antenna is well suited to radar applications and will continue to find applications in the future. Three relevant examples of radar applications well suited to the use of reflector antennas are briefly described below.

Low Cost Radar. For very cost-constrained applications where mechanical scan rates suffice, reflector antennas are still the dominant choice. One such niche is commercial weather radar, e.g., NEXRAD and TDWR.

Very High-Gain, Long-Range Radar. For very high-gain radar applications, the cost of an ESA is typically still prohibitive, and the reflector provides an economical means of realizing such high gains. Two examples of long-range radar applications generally requiring very high antenna gains are (1) missile defense radar and (2) space-based radar.

Limited Scan Radars. Some radars operate over a limited field-of-view and/or the requirements dictate fast electronic scanning over a small FOV and slower mechanical scanning over a larger field of view. ESA-fed reflector architectures are well suited for such applications and are described in greater detail in Section 12.3. Three relevant examples are (1) missile defense radar, (2) space-based radar, and (3) ground-based search and track radar (1D azimuth electronic scanning suffices for some of these applications).

Classification of Reflector Antennas. Radar reflector antennas can be classified in various ways. One useful classification criteria is electrical design, i.e., the reflector optics configuration. Table 12.1 provides a summary level comparison of some common radar

TABLE 12.1 Comparison of Key Features of Reflector Architectures

	Single Reflector Parabolic	Cylindrical Reflector	Dual Reflector (Cassegrain or Gregorian)	Confocal Paraboloids	Spherical and Torus
Electronic Scanning (Escan)	• Limited in both Azimuth and Elevation • Achieved via Feed switching	• Wide 1D scanning • Uses ESA line source for wide 1D scanning	• Limited in both Azimuth and Elevation • Achieved via feed switching	• Uses planar ESA source • Typically limited, but tradable by varying magnification	• Potential for very wide 1D scanning (torus) or 2D Scanning (spherical) • Achieved via feed switching
Aperture Efficiency Feed Type(s)	• Medium to high • No escan: Single horn • Escan: Array (switched feeds)	• Medium to high • 1D ESA line source	• High • No escan: Single horn • Escan: Array (switched feeds)	• High • 2D ESA planar source	• Modest to low • Switched beam array on circular arc (torus reflector) or spherical arc (spherical reflector)
Blockage Concerns	• Mitigate feed blockage via offset geometry	• Mitigate feed blockage via offset geometry	• Mitigate feed blockage via offset geometry • Can move feed behind reflector	• Mitigate feed blockage via offset geometry	• Serious concern for very wide scan configurations

reflector architectures from this perspective. More detailed discussions of the characteristics of these architectures are included in Section 12.3 wherein each of these architectures is afforded a dedicated subsection. Another means of classification is via platform (vehicle) or site (ground-based, ship-based, airborne, or space-borne). The platform frequently drives mechanical and environmental requirements and often either enables or constrains the reflector size. In Section 12.3, reflector architectures are discussed and compared, and in Section 12.6, mechanical and environmental design considerations are addressed.

Chapter Synopsis. The balance of this chapter is divided into five sections. Section 12.2 summarizes the basic design principles and parameters governing reflector antenna design. Section 12.3 provides a brief overview of conic sections and classes of reflector systems and associated optics. Section 12.4 discusses various types of reflector feeds and related design principles. Section 12.5 describes reflector analysis and synthesis methods and associated design software packages. Finally, Section 12.6 briefly reviews mechanical design issues and considerations.

12.2 BASIC PRINCIPLES AND PARAMETERS

Fundamentally, reflectors are antennas that work on optical principles, on receive, focusing energy to a focal point as a lens does for light. On transmit, power emanating spherically from a low gain, broad-patterned feed is reflected and energy is collimated to form a plane wave thereby providing increased antenna gain and a narrower beamwidth. In discussing antennas, one can use either transmit or receive arguments because antennas are reciprocal devices. This means that both the transmit and receive performance of a passive antenna, e.g., patterns, gain, losses, etc., can be predicted using basic aperture antenna principles. In this section, these basic reflector design principles are reviewed via use of a canonical example.

Consider a parabolic-shaped reflector forming a circular aperture, fed by a horn at a central focal point. This simple reflector configuration has a surface shape defined by the equation

$$z = \frac{x^2 + y^2}{4f} - f \tag{12.1}$$

where f is the focal length and the vertex is located at $z = -f$. The resultant antenna beam pattern points in the positive z-direction. For a round reflector of diameter D, the edge or rim is a circle and the edge dimensions are on this circle defined by

$$x_{\text{edge}}^2 + y_{\text{edge}}^2 = \frac{D^2}{4} \tag{12.2}$$

This reflector is shown in Figure 12.1.

One frequently is interested in the angle α from the z-axis to points on the reflector surface:

$$\alpha = 2 \arctan\left(\frac{\sqrt{x^2 + y^2}}{2f}\right) \tag{12.3}$$

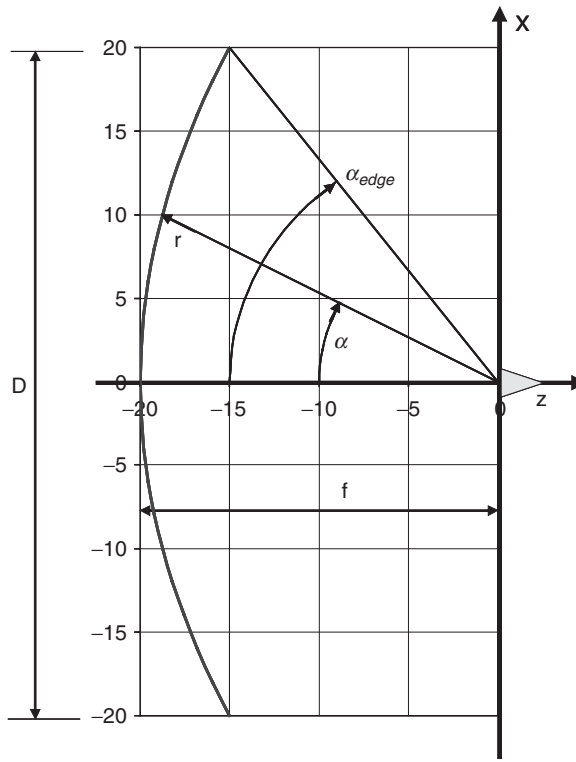

FIGURE 12.1 Parabolic reflector in *x*-*z* plane

Thus, the edge angle for a round reflector is

$$\alpha_{\text{edge}} = 2 \arctan\left(\frac{D}{4f}\right) \tag{12.4}$$

Another useful parameter is the distance r from the focal point to a point on the reflector:

$$r = f + \frac{x^2 + y^2}{4f} \tag{12.5}$$

Aperture Gain and Losses. The gain of the reflector antenna is one of its most important parameters. It is convenient to describe the reflector antenna gain with reference to the fundamental gain limit an aperture of area A. This limit, applicable to aperture antennas of sufficient electrical size (approximately 25 square wavelengths or greater), is the so-called aperture gain G_{ap},

$$G_{\text{ap}} = \frac{4\pi A}{\lambda^2} \tag{12.6}$$

where λ is the wavelength. For a round reflector of diameter D, this aperture gain limit is

$$G_{ap} = \left(\frac{\pi D}{\lambda}\right)^2 \tag{12.7}$$

In practice, it is sometimes useful to describe reflector gain by decrementing the aperture gain by subtracting various aperture radiation losses such as spillover, taper efficiency, feed blockage, reflector leakage, surface distortion, strut blockage, feed alignment, etc., from G_{ap}. These loss factors are described in detail later within this section.

Directive Gain and Feed Losses. Directive gain or directivity is a measure of the peak power relative to the average power radiated by an isotropic radiator, i.e., a radiator that radiates energy equally in all directions. Directive gain considers only the radiated power; thus, antenna losses such as feed mismatch, feed loss, and waveguide and/or cable losses must also be considered. However, the radar engineer typically tabulates these losses separately for use in other radar calculations. Antenna directivity is an imposing calculation requiring volume integrals, but typical reflector pattern computation codes express the pattern in terms of directivity, and the antenna losses are generally accounted for separately. In the text that follows, reflector directivity is described based upon available "aperture gain" and associated radiation losses. This approach should be intuitive to the radar engineer.

Aperture-Field Method of Analysis. The aperture-field reflector analysis method is based upon ray-tracing principles and works well for symmetric, center-fed parabolic reflectors. With this method, the aperture field distribution is calculated in an x-y plane at $z > 0$ (Figure 12.1) by assuming coherent reflection of spherical radiation from a feed at the focal point. The field distribution is then used to compute the far-field radiation pattern. For more complex geometries, e.g., offset-fed reflectors, this method does not work as well as the more rigorous physical optics (PO) method that is described in Section 12.4.

For the simple center-fed focal feed example shown in Figure 12.1, the simpler aperture-field method of analysis is accurate and its application is simple and straightforward and makes the discussion of the radiation losses easier to follow. Using this method of analysis, the field amplitude on an x-y grid, F_{grid}, in the aperture plane is easily determined from the feed and space tapering:

$$F_{grid}(x,y) = F_{feed}(x,y,z)\ \frac{f}{r} = \frac{F_{feed}(x,y,z)}{1+\dfrac{x^2+y^2}{4f^2}} \tag{12.8}$$

where F_{feed} is the feed radiation pattern. For this case, with the feed at the focal point, the total distance traveled from the feed to the reflector and back to the aperture-plane is equal. This expression is deceptively simple and accurately accounts for the feed-reflector transformations and area projections.[1,2]

The resultant aperture field, $F(\hat{v})$, is then transformed to the far field using the spatial transformation:

$$F(\hat{v}) = \sum_{x,y} F_{grid}(x,y)\ \ e^{j\frac{2\pi}{\lambda}\left(x\hat{i}_x + y\hat{i}_y\right)\bullet\hat{v}} \tag{12.9}$$

where $\hat{v}$ is a unit vector in the direction of interest. Note that Eq. 12.9 is a simple 2D spatial summation analogous to that used for array antenna pattern calculations.

Taper Efficiency. In antenna design, aperture taper is used to lower sidelobes. The modest resultant loss and increased beamwidth is the price and one is usually willing to pay to obtain the desired sidelobe level. The loss associated with aperture taper is accounted for in the taper efficiency. However, the taper efficiency is not an ohmic loss where energy is dissipated, but is a redistribution of energy. In the case of a reflector fed by a horn, the taper distribution is determined by the feed horn pattern, the distance to the reflector, and the projected area in the direction of peak radiation. For a radially symmetric feed and reflector, where the field is radially symmetric and $F_{\text{grid}}(x,y) = g(r)$, the efficiency, η, is computed as

$$\eta = \frac{\left|\int g(r)\ 2\pi r\, dr\right|^2}{\int g^2(r)\ 2\pi r\, dr \int 2\pi r\, dr} \tag{12.10}$$

Spillover Loss. Spillover loss refers to feed power that misses, or spills over, the edges of the reflector. In the radar reflector design process, one typically adjusts the edge illumination to achieve a desired taper and sidelobe level resulting in modest spillover loss. Spillover loss is the feed power that is lost via radiation beyond the edges of the reflector. This loss can be computed as

$$\text{Spillover Loss} = \text{Total Feed Power}\left(1 - \frac{\text{Feed Power Incident on Reflector}}{\text{Total Feed Power}}\right) \tag{12.11}$$

For a radially symmetric feed and reflector, this calculation is straightforward.

Edge diffraction and resultant antenna backlobes are a related consequence of feed spillover and edge taper. For any given reflector design, edge illumination of the reflector will produce radiation behind the reflector due to diffraction. This diffraction may be thought of as re-radiation from the edge of the reflector that causes radiation lobes behind the reflector. For a center-fed reflector such as that shown in Figure 12.2, a primary backlobe will arise directly behind the reflector due to coherent addition of the edge diffraction currents. One common means of specifying this backlobe level is via the front-to-back F/B ratio, i.e., the ratio of the main beam and backlobe gains. The analysis of these reflector edge diffraction effects and associated F/B ratios for some common reflector geometries are described by Knop.[3]

Feed Blockage.[4,5] Many reflector systems suffer feed and/or feed-support blockage to some degree. For center-fed geometries, there will definitely be blockage because the feed is within the FOV of the reflector. A consequence of blockage is higher sidelobes, the levels of which depend upon the blockage area. Another consequence is loss due to blockage and depends upon the blocked electric field to main electric field ratio, E_b/E_m, which, in turn, is determined from the ratio of blocked power to total power on the main reflector, P_b/P_m, and ratio of the gain of the blocking object to the gain of the main reflector, G_b/G_m:

$$\left(\frac{E_b}{E_m}\right)^2 = \frac{P_b}{P_m}\ \frac{G_b}{G_m} \tag{12.12}$$

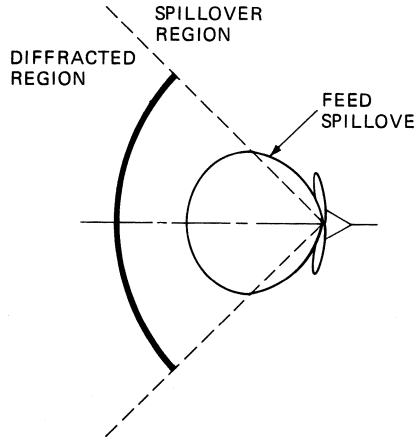

FIGURE 12.2 Graphical representation of spillover loss

Reflector taper is often approximated by a radial amplitude distribution[4]

$$g(r) = 1 - r^2 \tag{12.13}$$

where r is the radial distance normalized to the reflector radius and $g(r)$ drops to zero at the edge. The use of this taper function leads to a simple blockage loss equation:

$$\frac{P_b}{P_m} = \frac{g^2(0)\int_0^1 2\pi r\,dr}{\int_0^1 g^2(r)\,2\pi r\,dr}\,\frac{D_b^2}{D_m^2}$$
$$\frac{G_b}{G_m} = \frac{D_b^2}{\eta\,D_m^2} \tag{12.14}$$

where η is the efficiency, as given in Eq. 12.10. Using Eq. 12.14 and Eq. 12.15 leads to the simple expression for blockage loss typically found in the literature[5]:

$$\frac{E_b}{E_m} = 2\,\frac{D_b^2}{D_m^2}$$
$$\text{Blockage Loss} = \left(1 - \frac{E_b}{E_m}\right)^2 = \left(1 - 2\,\frac{D_b^2}{D_m^2}\right)^2 \tag{12.15}$$

where D_b and D_m are the diameter of the blockage and reflector, respectively.

The effective feed horn dimensions causing blockage may be different from the physical dimensions. If the walls are not tapered, such as shown in Figure 12.3, the effective size of the blockage hole can be larger than the projected obstacle area.

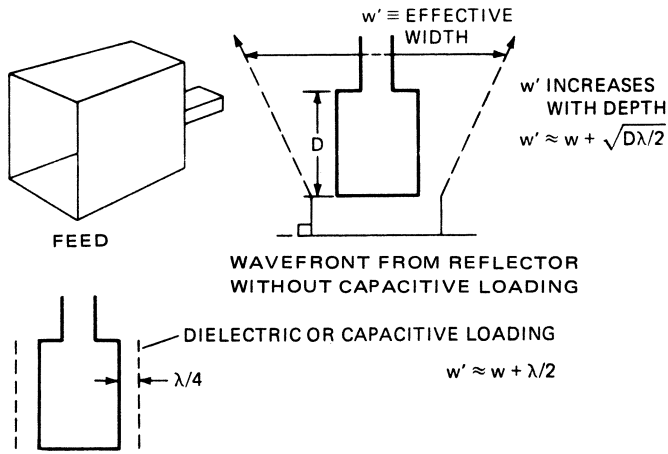

FIGURE 12.3 Capacitive loading to reduce feed horn blockage

For feeds with conducting walls, the effective H-plane width, w', is at least $\lambda/4$ and increases with depth D:

$$w' = w + \max\left\{\lambda/4, \sqrt{\lambda D/2}\right\} \tag{12.16}$$

where max indicates taking the larger of the two values. The increase in effective width can sometimes be reduced by adding capacitive loading, which can constrain the effective width to about a quarter wavelength wider than the physical width. The effective E-plane dimension is the same as the actual dimension.

Gain Optimization. Three of the principal reflector antenna losses, taper efficiency (loss), spillover, and blockage, have been explained in detail above. These design parameters (loss factors) affect one another and are often traded to optimize antenna performance, e.g., gain, sidelobes, etc. Other typical reflector losses, described later in this section, are resistive loss factors that simply reduce the antenna gain.

The design trades associated with taper efficiency, spillover, and blockage are illustrated by use of an example. Computed losses are shown in Figure 12.4 for a 20-wavelength diameter center-fed circular reflector with a 10-wavelength focal length, and a gaussian feed horn (a horn with a radiation pattern described by a gaussian function). The gaussian feed used in this sample analysis is a hypothetical feed with a radially symmetric pattern and very low spillover, and most typical feed horn patterns are well approximated by a gaussian feed model. The feed size determines the edge taper, i.e., the larger the feed, the greater the edge taper. The plot in Figure 12.4 shows how the three loss terms, and the total loss, vary as a function of feed pattern edge taper, that is, the feed power directed at the edge of the reflector, relative to the feed pattern peak. This is used here because the feed pattern is measured independent of the reflector. When the edge taper is low, virtually all the power strikes the reflector and the loss is insignificant. As taper decreases, there is more spillover, and feed power misses the reflector, increasing the loss. On the other hand, with too much taper, the taper efficiency is poor because the reflector is under illuminated.

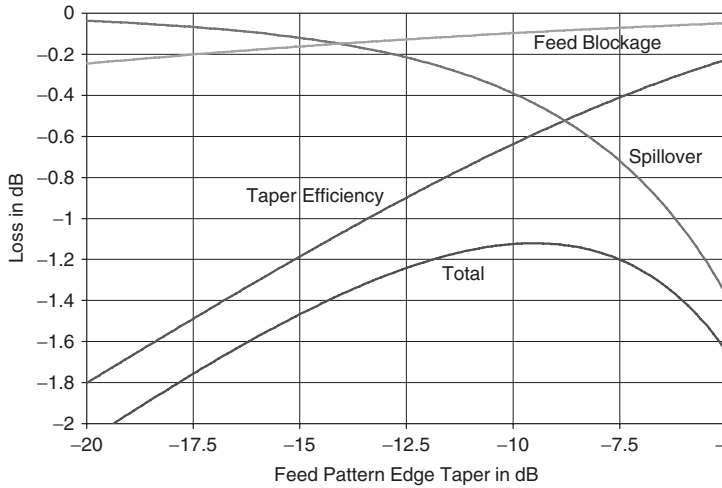

FIGURE 12.4 Taper efficiency, spillover, blockage, and total loss vs. feed pattern edge taper

Figure 12.4 demonstrates the gain optimization process with a hypothetical feed pattern, blockage, etc., and the total loss is 1.11 dB (77% efficiency) when a –9.5 dB edge taper is implemented. Although the plot of Figure 12.4 includes taper, blockage, and spillover losses, there are additional losses that must be included when assessing the overall aperture efficiency. These losses, e.g., feed blockage, surface reflection, feed mismatch, and resistive losses, etc., vary from system to system, but 0.8 dB is typical. With these additional losses, the overall loss becomes 1.91 dB or 64% aperture efficiency (typical for a single reflector system).

Sidelobe requirements must also be considered. As shown in Figure 12.5, for the same center-fed reflector system, the sidelobe level can be reduced by increasing the feed pattern edge taper.

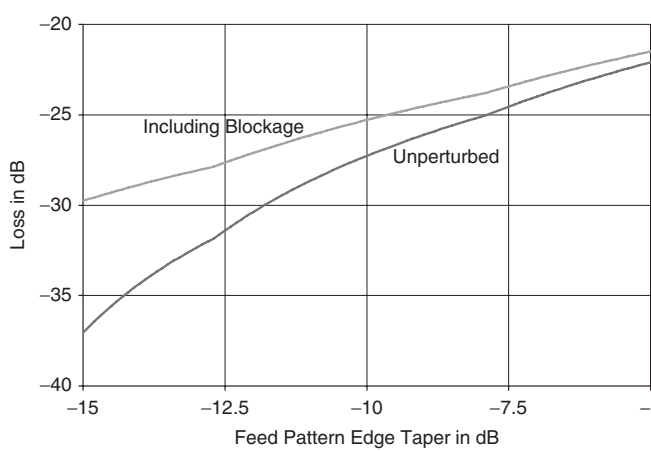

FIGURE 12.5 Sidelobe levels, with and without blockage, vs. feed pattern edge taper

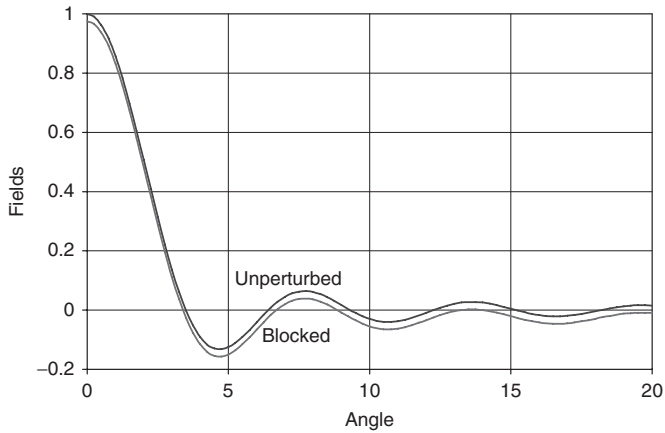

FIGURE 12.6 Unperturbed field and field including feed blockage

Figure 12.5 also shows that feed blockage increases the sidelobe level; for example, with a –10 dB edge taper, one obtains –25.5 dB sidelobes rather than –27.5 dB sidelobes. Figures 12.6 and 12.7 further illustrate this impact. This blockage effect can be modeled as a "hole" in the aperture that can be represented by a broad pattern with less gain. This blockage pattern is subtracted from unperturbed (unblocked) aperture fields, as shown in Figure 12.6.

The associated patterns, with and without blockage, are shown in Figure 12.7. The alternating large, small, large, and so on, sidelobe progression is characteristic of a blocked aperture.

Surface Leakage Loss. Many reflector surfaces are designed with a grid, a wire-mesh, or metalized fabric surface in order to minimize wind resistance, reduce weight, and/or enable stowage/deployment. Some common reflector mesh surface patterns are

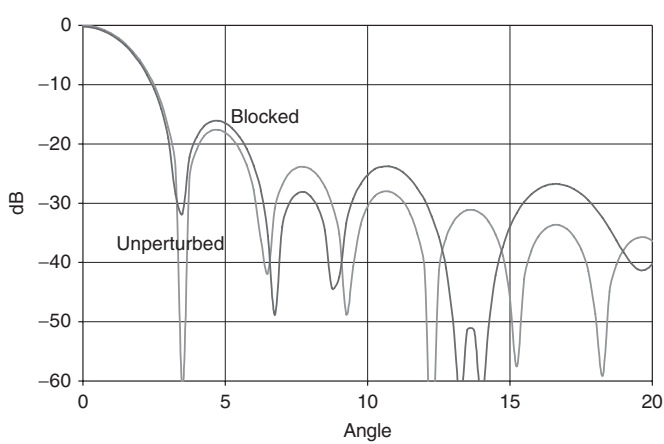

FIGURE 12.7 Unperturbed pattern and pattern including blockage

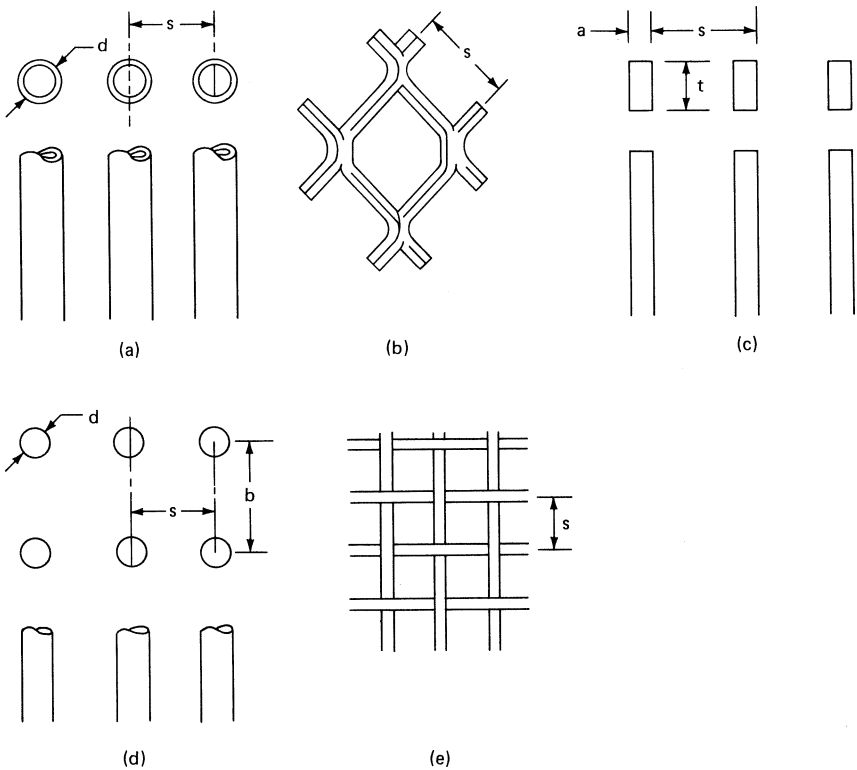

FIGURE 12.8 Common reflector surface materials for reduced wind resistance: (*a*) tubing, (*b*) expanded metal, (*c*) rectangular, (*d*) double layer, and (*e*) screen

shown in Figure 12.8. The mesh opening size is generally chosen to be as large as possible, but the gap, s, between conductors must be substantially less than $\lambda/2$ to cutoff and prevent significant transmission of electromagnetic energy through the surface. The attenuation, in decibels, through the passage depth t is approximately $27t/s$, plus fringing losses, which are approximately $27(\lambda/2s - 1)$.

The power passing through the reflector, or transmission loss, can be determined using a handy nomograph.[6] One selects the grid spacing and thread radius to achieve the transmission loss required. The resulting loss in antenna gain is termed *leakage loss*, and the relationship between leakage loss and transmission loss is plotted in Figure 12.9 for a conductive reflector (no ohmic losses). The leakage loss vs. spacing relationship for Figure 12.8*a* can also be computed using an equivalent circuit, with shunt susceptance, b, developed by Mumford,[7] the source of the nomograph[6]:

$$b = -\frac{\lambda}{s \ln\left(\dfrac{0.83}{1 - e^{-\pi d/s}}\right)} \qquad \text{Leakage Loss} = \frac{1}{1 + b^2/4} \tag{12.17}$$

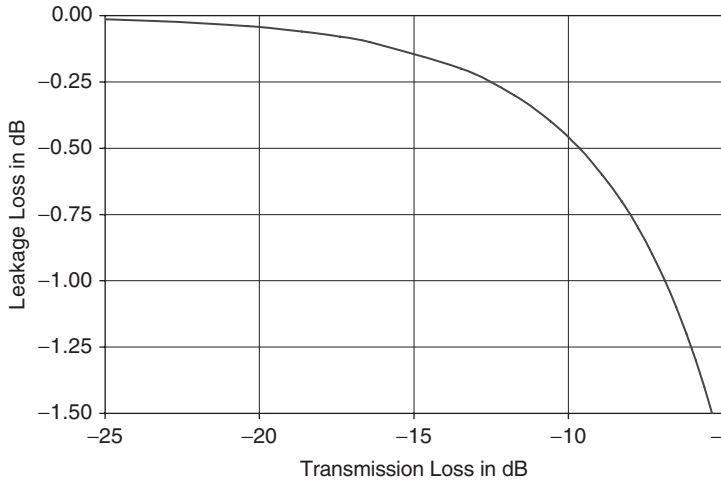

FIGURE 12.9 Reflector leakage loss vs. transmission loss

This nomograph[6] is frequently used for the simple configurations in Figure 12.8*a*. For other configurations and thread forms, the same equation can be used by computing an equivalent radius by matching the cross sectional areas.

One significant source of radiation in the back hemisphere is leakage through the reflector. This radiation level is determined from the difference between primary (feed horn) and secondary (reflector) gains and the leakage (loss) radiation through the mesh.

There are two considerations regarding the reflector surface leakage. The leakage loss affects the reflector gain directly. The radiation level in the back hemisphere is a function of the feed gain, reduced by the transmission loss through the reflector. Thus, the reflector designer must consider both the leakage loss and the transmission loss (Figure 12.9).

There are, however, additional backlobes that are distinct from the back radiation due to surface leakage. These additional lobes are due to reflector edge diffraction that adds coherently and typically causes a relatively strong main backlobe behind the reflector. Center-fed geometries, i.e., those with reflector edges equidistant from the feed, enable coherent addition of the diffracted energy directly to the rear of the reflector. For these geometries, the backlobe level is directly related to the edge illumination level.[3]

Surface Roughness Loss. All radar reflector antennas, especially those that are mechanically scanned or deployed, require careful consideration of mechanical design details. First, the reflecting surface must be designed and built so that it remains within close tolerances (typically $\pm 0.03\lambda$) even under dynamic operating and environmental conditions. Also, the feed must be accurately aligned with respect to the reflector. The feed-support structure and the reflector stiffening structure must maintain the feed location and surface dimensions while the antenna is being rotated. This dimensional stability must be maintained through wind loading, temperature variations, or other environmental factors to ensure that pattern performance is maintained.

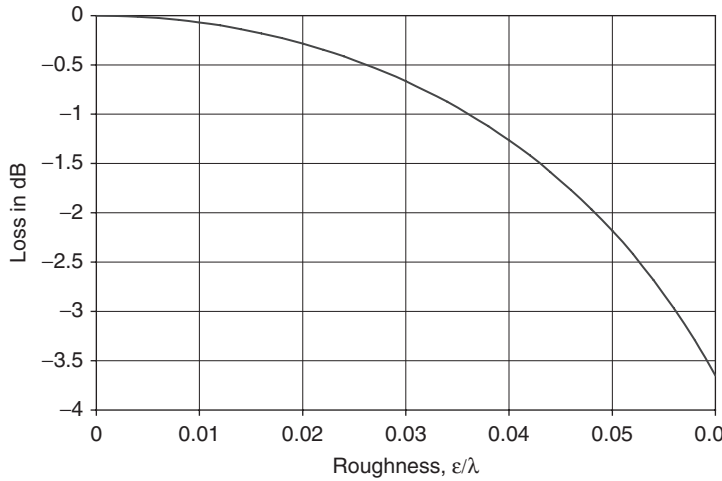

FIGURE 12.10 Surface roughness, ε/λ, vs. loss

Reflector antenna gain loss due to surface roughness has been discussed by John Ruze[8,9] using a statistical point of view. The loss of gain due to small roughness errors is approximately[9]

$$\frac{G}{G_0} \approx 1 - \overline{\delta^2} = 1 - \left(\frac{4\pi\varepsilon}{\lambda}\right)^2 \tag{12.18}$$

where $\overline{\delta^2}$ is the mean square phase error, ε is the effective rms surface error, λ is the wavelength, G_0 is the gain without phase error, and G is the gain with phase error.

The roughness loss effects embodied in Eq. 12.18 are captured in Figure 12.10 where gain loss vs. surface roughness (in lieu of phase error) is plotted. The plot shows that for 0.10 dB gain loss, the rms surface error must be less than 0.01λ. To maintain modest losses, surface errors must be tightly controlled.

Another consideration in mesh reflectors is systematic surface deformation. For many reflectors, a mesh is attached to a metal or composite backing structure. For spaceborne deployable reflectors, the mesh is typically a very sheer fabric-like membrane that is stretched across the surface and attached at a finite number of points to form the reflecting surface. In either case, there are surface distortions between the precisely controlled mounting points. This sets up a systematic error in the form of periodic cusps (see Figure 12.11). These errors typically cause pattern grating lobes because these error cusps are normally several wavelengths apart. The grating lobes are easily recognizable based on their

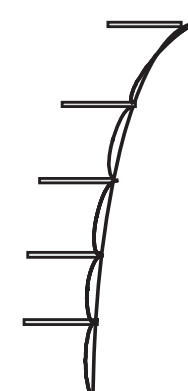

FIGURE 12.11 Systematic displacement between supports with a cusp between supports

well-defined angular spacing. For a grid with supports, and associated errors, a distance s apart, the grating lobe appears at

$$\theta = \arcsin(s/\lambda) \tag{12.19}$$

The grating lobe amplitude depends on the depth of the distortion (Figure 12.11), and is typically

$$\text{Grating Lobe} = \left(\frac{4\pi\varepsilon}{\lambda}\right)^2 \tag{12.20}$$

where ε is the depth of the cusp.

Feed Displacement. The permissible total error in the overall feed-reflector system alignment[10–12] is generally restricted to $\lambda/8$ or $\pm\lambda/16$. On the basis of this criterion, the resultant maximum deviation from the parabolic condition (feed at focus) would be $\pm\lambda/32$. Displacement of the feed along the focal axis (the z-axis in Figure 12.1) produces an even-order phase error on the aperture illumination. This results in modest beam broadening and some filling of the first null, but is normally not too detrimental.

Displacement of the feed normal to the z-axis produces an odd-order phase error in the aperture and causes higher sidelobes on one side of the beam. Furthermore, such displacement will cause the beam to mispoint. If the displacement is small, fixed, and known, one can typically calibrate out the fixed mispointing bias. However, if the displacement is random, say caused by vibration, the beam pointing error can be a problem. The reflector beam will be steered by θ radians if the feed is displaced off axis by an amount ε

$$\theta = \arctan(\varepsilon/f), \text{ radians} \tag{12.21}$$

where f is the focal length. So if the lateral feed displacement error is ε, the beam pointing error, $\Delta\theta$, is

$$\Delta\theta = \frac{\varepsilon/f}{1+(\varepsilon/f)^2}, \text{ radians} \tag{12.22}$$

Strut Blockage. Struts are used to support the feed, and for center-fed reflectors, typically form a tripod, as shown in Figure 12.12. Strut scattering is a complex phenomena that depends on strut size, strut geometry, field polarization, and other factors. However, in general, strut interference scattering will lie within a conical region about the strut axis. The strut is illuminated by a planar wavefront and one edge of the scattering cone lies on the reflector axis (see Figure 12.13). If the strut tilts at 30° to the axis, the scattering cone maximum angle is twice the tilt angle, or 60°. Thus, the scattering from three struts forms intersecting rings, as shown in Figure 12.14. This causes the most blockage at the pattern peak where the three rings intersect.

Polarization plays a significant role in strut scattering. For the example shown in Figure 12.12, strut #1 is parallel to the E-field and its blockage area is larger than its actual physical cross section. However, the lower struts, #2 and #3, are tilted 60° with respect to the E-field, and therefore appear smaller than their physical cross section.

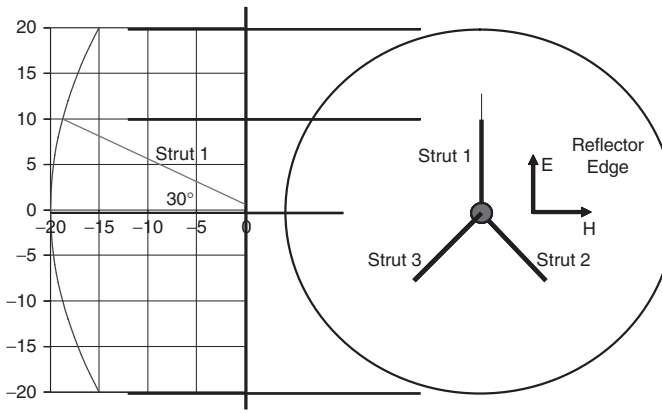

FIGURE 12.12 Center-fed reflector with tripod struts, side view, and axial view

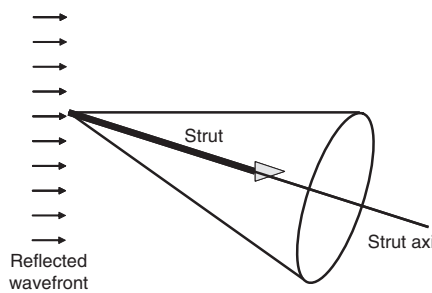

FIGURE 12.13 Strut 1 and maximum scattering cone

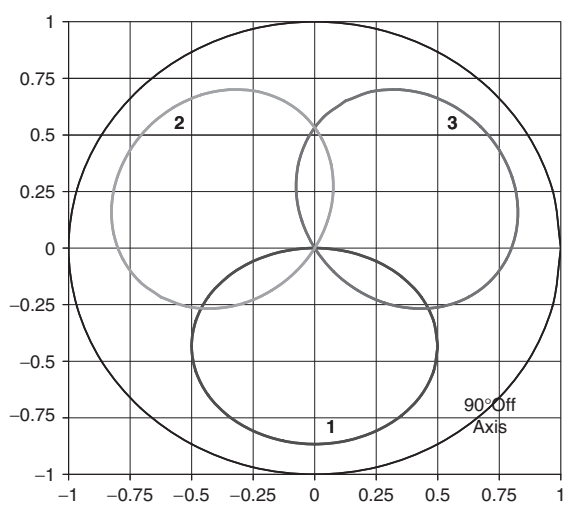

FIGURE 12.14 Axial view of 30° tripod strut blockage interference patterns

12.3 REFLECTOR ANTENNA ARCHITECTURES

Reflector antennas are built in a wide variety of shapes and sizes with a corresponding variety of feed systems to illuminate the surface(s), each suited to its particular application. Figure 12.15 illustrates the most common of these reflectors, each of which is described in some detail in the following subsections. The paraboloid in Figure 12.15*a* collimates radiation from a feed at the focus into a pencil beam, providing high gain and minimum beamwidth. The parabolic cylinder in Figure 12.15*b* performs this collimation in one plane but allows the use of a linear array in the other plane, thereby allowing flexibility in either steering or shaping of the beam in that plane. If beam shaping (not scanning) is the goal, an alternative method using a single feed, in lieu of a linear array, is shown in Figure 12.15*c*. Shaping of the surface along the vertical axis is used to spoil the beam shape in this plane, but because only the phase of the wave across the aperture is changed, there is less control over the beam shape than in the parabolic and/or phase cylinder shown in Figure 12.15*b* wherein the linear array may be adjusted in amplitude.

Very often the radar designer needs multiple beams to provide increased coverage or to determine angle. Figure 12.15*d* shows how multiple discrete feed locations produce a set of secondary beams at distinct angles. The additional feeds must be offset from the focus, and the resultant secondary beams will suffer some gain loss and distortion commensurate with the associated feed displacement. If an ESA feed is used, the reflector system can be designed to enable electronic beam scanning, albeit over a limited FOV. The use of modern ESA and ESA-like reflector feeds to achieve electronic scanning is discussed further in Section 12.4. An especially common multiple beam design is the monopulse antenna in Figure 12.15*e*, used for angle determination on a single pulse, as the name implies. In this instance, the second beam is normally a difference beam with its null at the peak of the first beam.

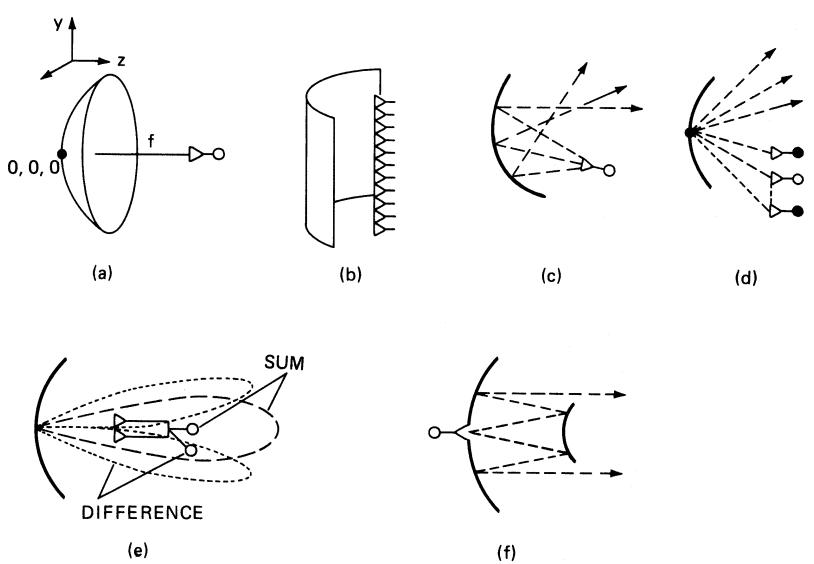

FIGURE 12.15 Common reflector antenna types: (*a*) paraboloid, (*b*) parabolic cylinder, (*c*) shaped, (*d*) stacked beam, (*e*) monopulse, and (*f*) Cassegrain

Multiple reflector systems, typified by the Cassegrain antenna shown in Figure 12.15*f*, offer one more degree of flexibility by shaping the primary beam and/or allowing the feed system to be conveniently located behind the main reflector. The symmetrical arrangement shown has significant blockage, but offset geometries mitigate feed blockage.

In modern reflector antenna design, combinations and variations of these basic types are widespread; however, design goals generally stress beam gain(s), shape(s), location(s), etc., while stipulating minimal losses and low sidelobe levels.

Paraboloidal Reflector Antennas. The theory and design of paraboloidal reflector antennas are extensively discussed in the literature.[13–17] A basic geometry is shown in Figure 12.16*a*, which assumes a parabolic reflector surface of focal length f with a feed at the focal point. It can be shown from geometrical optics considerations that a spherical wave emerging from the focal point, F, and incident on the reflector is transformed, after reflection, into a plane wave traveling in the positive z direction (Figure 12.16*b*).

Although reflectors are commonly illustrated with a round outline or rim and a central feed point, a variety of reflector aperture shapes are used in practice, as shown in Figure 12.17. Often, the azimuth and elevation beamwidth requirements differ, requiring an oblong aperture, as shown in Figure 12.17*b-e*.

If low sidelobe levels are required, feed blockage may become intolerable, requiring the use of an offset feed (Figure 12.17*c*). The feed is still generally located at the focal point, but the reflector is realized via use of a different portion of the parabola. For offset-fed reflector configurations, the focal axis generally does not intersect the reflector surface. Feeds for offset-fed reflectors are generally aimed close to, but slightly beyond, the center of the reflector area to account for the larger space taper (spreading loss) on the far side of the reflector. This generally results in a slightly unsymmetrical aperture illumination.

The corners of most paraboloidal reflectors are frequently rounded (not shown) or mitered (Figure 12.17*d*) to reduce extraneous surface area and/or minimize the torque required to turn the antenna. Because these corner regions are generally weakly

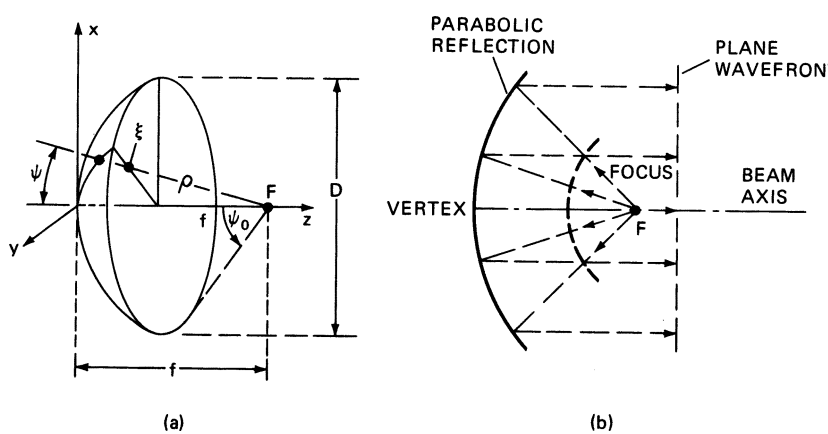

FIGURE 12.16 Geometrical representation of a paraboloidal reflector: (*a*) geometry and (*b*) operation

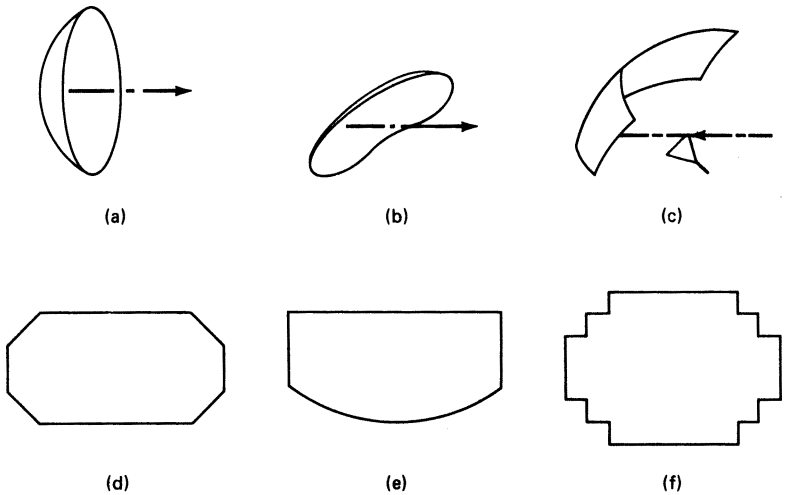

FIGURE 12.17 Paraboloidal reflector aperture shapes or rims: (*a*) round outline/rim, (*b*) oblong, (*c*) offset feed, (*d*) mitered corner, (*e*) square corner, and (*f*) stepped corner

illuminated by the feed, their removal generally has little impact on the gain. However, circular and elliptical outlines/rims will produce modest sidelobes in both principal and nonprincipal planes. If very low sidelobes are specified in nonprincipal planes, it may be necessary to maintain square corners, as shown in the upper part of Figure 12.17*e*.

Parabolic-Cylinder Antenna.[18,19] It is quite common that either the beam must be steerable or shaped in only one plane, either azimuth or elevation. A parabolic cylindrical reflector fed by a linear array feed can accomplish this at moderately higher cost.

The parabolic cylinder antenna can be applied to achieve a precisely shaped beam from a common aperture. The AN/TPS-63 (Figure 12.18) uses a vertical array to provide fine control of the elevation pattern with a single elevation column feed array and so is very cost effective. The elevation beam-shaping incorporates a steep beam slope at the horizon to allow radar operation at low elevation angles without degradation from ground reflections. The TPS-63 produces a much sharper slope at the horizon than a shaped reflector of equal height. The array feed enables superposition of beams close to the aperture normal, thereby enabling very high taper efficiency (near full aperture gain).

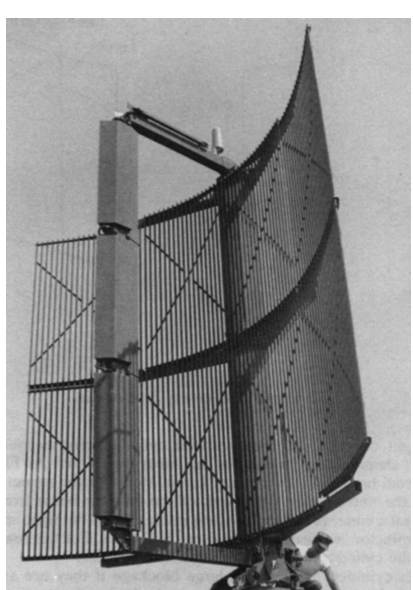

FIGURE 12.18 AN/TPS-63 parabolic-cylinder antenna (*Courtesy Northrop Grumman Corporation*)

The basic parabolic cylinder geometry is shown in Figure 12.19. The reflector surface is defined as

$$z = \frac{y^2}{4f} - f \tag{12.23}$$

where z is the distance from the focal plane, f is the focal length of the cylindrical reflector, and y is the horizontal dimension. For the parabolic cylinder, the surface does not vary with x, the height. The feed is generally on the focal line, and in many ways, the design of parabolic cylinder reflectors is similar to that of paraboloidal reflectors. One significant difference is that the feed energy diverges cylindrically rather than spherically, and so the feed power density falls off as $1/\rho$ rather than $1/\rho^2$.

The height of the parabolic cylinder (Figure 12.19*a*) must allow for beamwidth, shaping, and steering of the linear feed array. When the line source steers at angle θ from broadside, the primary beam from the source lies on a conic, and the intercepts at the upper right and left corners of the reflector are farther up than in the center, as shown in Figure 12.19*b*. Therefore, the corners of parabolic cylinder reflectors are seldom rounded in practice.

Shaped Reflectors. Fan beams with a specified shape are required for a variety of reasons. A common elevation shaped beam requirement is to provide equal echo signal power on targets at constant altitude. If the transmit and receive beams are identical, and if secondary effects are ignored, this can be achieved with a power radiation pattern proportional to $\csc^2\theta$, where θ is the elevation angle.[13] In practice, the well-known cosecant-squared pattern is typically modified to account for the curvature of the earth and the characteristics of sensitivity time control (STC).

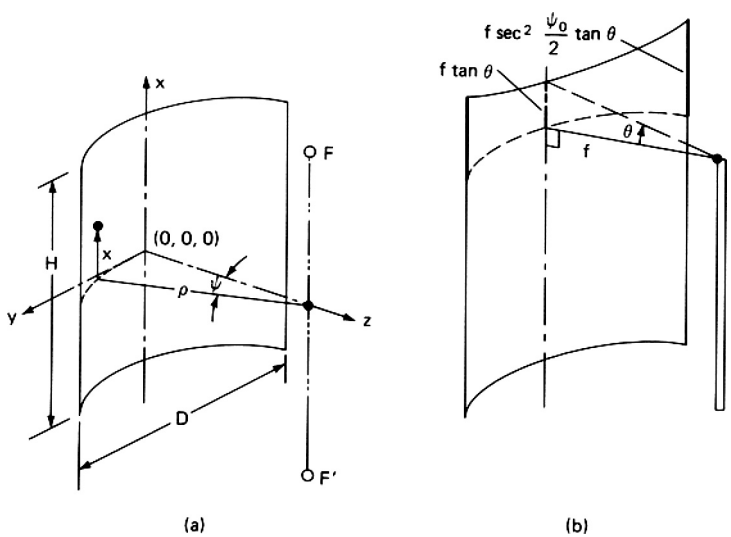

FIGURE 12.19 Parabolic cylinder: (*a*) geometry and (*b*) surface extension enables line source steering.

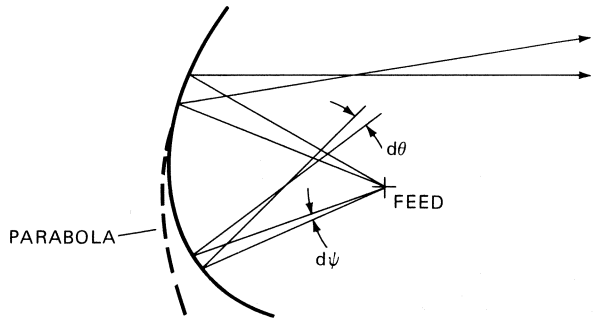

FIGURE 12.20 Reflector shaping

A relatively simple way to shape the beam is to shape the reflector, as Figure 12.20 illustrates. Each portion of the reflector is designed to reflect a portion of the incident energy in a different direction, and to the extent that geometric optics is valid, the power density at that angle is the integrated sum of the power density from the feed across that portion of the reflector. Silver[13] graphically describes a procedure for determining the reflector contour for a cosecant-squared beam. However, computer software packages now exist that enable synthesis of arbitrary beam shapes via application of iterative optimization techniques in conjunction with physical optics–based pattern computations. These analysis methods and software packages are summarized in Section 12.5.

Offset-fed parabolic reflectors are often used to mitigate feed blockage. However, reflector shaping can also be used to mitigate blockage and is sometimes applied to redirect the reflected energy away from the feed, as shown in Figure 12.20. Figure 12.21 illustrates how shaping can be applied to virtually eliminate blockage even though the feed appears to be within the FOV of the reflector.

The ASR-9 antenna (Figure 12.22), found at major airports, typifies shaped reflector antenna design. The elevation beam shape is tailored using a computer-aided design process, and azimuth sidelobes are lowered by offsetting the feed so there is no blockage. Two linear or circularly polarized elevation beams are produced by using two feedhorns. One beam is close to the horizon for close in targets, and the second is higher in elevation, so it receives less ground clutter for long range targets.

One typical characteristic of shaped reflectors is lower aperture efficiency. Generally, the surface shaping process spoils the aperture phase and broadens the beam thereby inherently reducing the aperture efficiency. However, this sacrifice in aperture efficiency is generally accepted by the radar designer when beam shaping is desired or required.

The second antenna atop the ASR-9 reflector (Figure 12.22) provides an independent tracking system. It is an Air Traffic Control Radar Beacon System array antenna that transmits and receives narrow azimuth sum, difference, and guard beams, all shaped in elevation. It requires a transponder aboard the aircrafts targeted, as it has low gain.

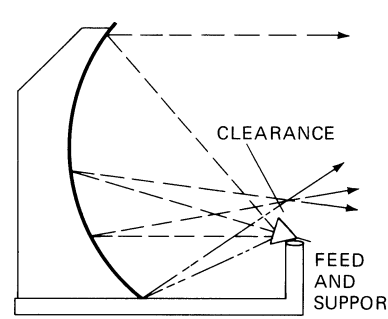

FIGURE 12.21 Elimination of blockage

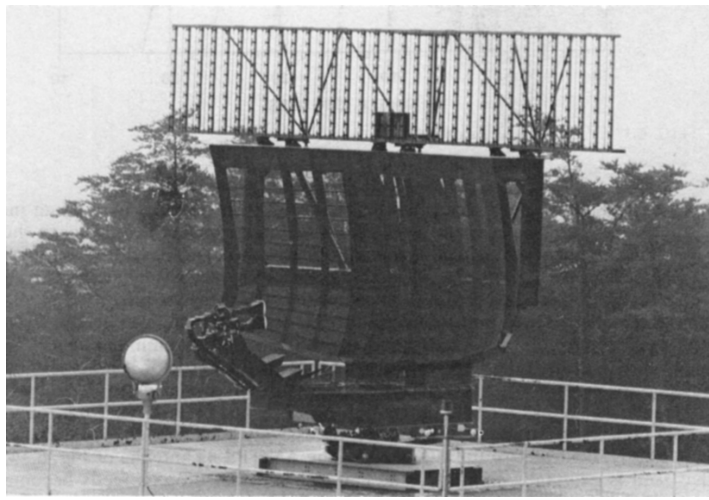

FIGURE 12.22 ASR-9 shaped reflector with offset feed. Air Traffic Control Radar Beacon System (ATCRBS) array is mounted on top. (*Courtesy Northrop Grumman Corporation*)

Multiple-Reflector Antennas.[20–30] There are both difficulties and advantages associated with adding a secondary, or subreflector, to a paraboloidal reflector system. The shape of the subreflector determines how the power will be distributed across the primary reflector and thereby provides some control over amplitude in addition to phase in the aperture, making it possible to produce very low spillover or to produce a specific low-sidelobe distribution. By suitable choice of shape, the apparent focal length can be enlarged so that the feed size is practical or even feasible. This is sometimes necessary for monopulse operation.

The Cassegrain dual reflector antenna (Figure 12.23), derived from optical telescope designs, is the most prevalent dual reflector configuration. Figure 12.23*a* shows a small subreflector between the feed and parabolic main reflector. The feed illuminates the hyperboloidal subreflector, which in turn illuminates the paraboloidal main reflector. The feed is placed at one focus of the hyperboloid, and the paraboloid focus is coincident with the second focus of the hyperboloid. The use of a subreflector also allows the feed to be located behind the main reflector and closer to the transmitter and receiver in order to minimize transmission line losses. Furthermore, if the feed is located behind the main reflector, the center of gravity will be biased closer to the main reflector vertex thereby simplifying the design of both the structure and the gimbal (precision mechanical positioning system).

The Gregorian dual reflector antenna system (not shown in Figure 12.23) is similar to the Cassegrain, but it uses an ellipsoidal subreflector in lieu of a hyperboloid resulting in a lengthening of the reflector system (along the focal axis).

The parameters of the Cassegrain reflector[20] are related by the following expressions:

$$\begin{aligned} \tan \psi_v/2 &= 0.25 D_m/f_m \\ 1/\tan \psi_v + 1/\tan \psi_r &= 2f_c/D_s \\ 1 - 1/e &= 2L_v/f_c \end{aligned} \tag{12.24}$$

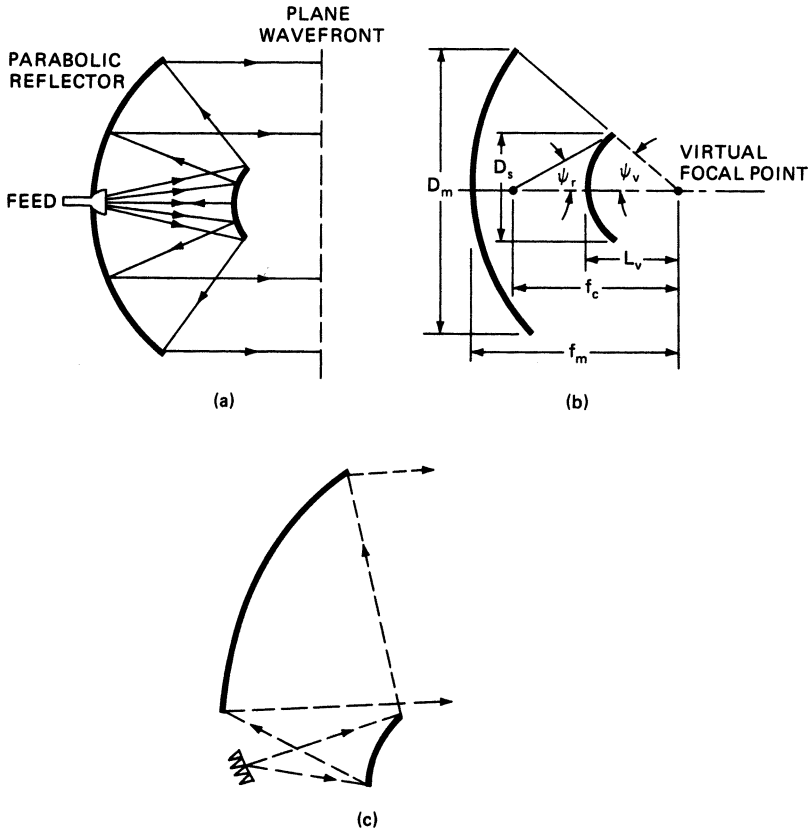

FIGURE 12.23 Cassegrain dual reflector antenna systems (the larger surface is the main reflector and the smaller surface is the subreflector): (*a*) ray optics (*b*) typical axial configuration,[20] and (*c*) offset configuration

where the eccentricity e of the hyperboloid is given by

$$e = \sin[(\psi_v + \psi_r)/2]/\sin[(\psi_v - \psi_r)/2]$$

The equivalent-paraboloid[20] concept is a convenient method of analyzing the radiation characteristics using a single reflector "equivalent" model. This method utilizes a paraboloid of equal diameter, but a larger focal length to model the dual-reflector Cassegrain system. The equation

$$f_c = D_m/(4\tan(\psi_r/2)) \tag{12.25}$$

defines the equivalent focal length, and the focal length ratio or magnification m is given by

$$m = f_c/f_m = (e+1)/(e-1) \tag{12.26}$$

The magnification m is a useful metric in that it provides a measure of the reduction in size/length along the focal axis that is enabled by use of the Cassegrain reflector system in lieu of a single parabolic reflector system. The feed is designed to produce suitable illumination within subtended angles $\pm\psi_r$ associated with the longer focal length f_c.

Aperture blocking can be large for center-fed Cassegrain antennas. The blockage can be minimized by choosing the diameter of the subreflector to be equal to that of the feed.[20] This occurs when

$$D_S = \sqrt{2f_m\ \lambda/k} \tag{12.27}$$

where k is the ratio of the feed-aperture diameter to its effective blocking diameter. Ordinarily k is slightly less than 1. For linearly polarized radar applications, aperture blocking can be significantly reduced by using a polarization-twist reflector and a subreflector made of parallel wires.[24] This twist reflector design enables a 90° rotation of the polarization such that the polarization of the beam upon reflection from the main reflector is orthogonal and transparent to the gridded subreflector.

Blockage can also be eliminated by offsetting both the feed and the subreflector (Figure 12.23*c*). With blockage and supporting struts and spillover virtually eliminated, this geometry is useful for very low sidelobe applications.[24]

As described earlier, the aperture efficiency of single reflector systems is maximized by balancing the feed taper and the feed spillover and minimizing other losses, but is typically 55–65%. However, dual reflector systems (e.g., Cassegrain) have an additional degree of freedom and surface shaping can be applied to decrease the taper loss and enable aperture efficiencies in excess of 70%.[25,26]

A different type of dual reflector system that is particularly well-suited to applications where limited electronic scanning is required is the so-called confocal reflector system[27–30] shown in Figure 12.24. This system employs two parabolic reflectors, a main and a sub, that share a common focal point. The optics of this system is designed such that a plane wave source, say from an array, is first converted to a spherical wave at the subreflector. Then, upon reflection from the subreflector, the feed energy converges at the common focus and diverges again as a spherical wave before finally reflecting from the main reflector.

The confocal system has several interesting properties, tied to the magnification factor M:

$$M = f_M / f_S \tag{12.28}$$

where f_M and f_S are the focal lengths of main and subreflectors, respectively. The first property shows that the system is essentially a feed source magnifier. The reflector gain, G_r, is described by

$$G_r \approx G_f \times M^2 \times \cos(\theta_r) \tag{12.29}$$

where G_f is the gain of the feed array and θ_r is the scan angle of the reflector (secondary) beam. The second property defines the scanning. The reflector scan angle, θ_r, is defined by the following equation:

$$\theta_r \approx \theta_f/M \tag{12.30}$$

where θ_f is the feed scan angle. For example, if the magnification factor is 10 and the ESA feed array is scanned 30°, the reflector beam will scan approximately 3°.

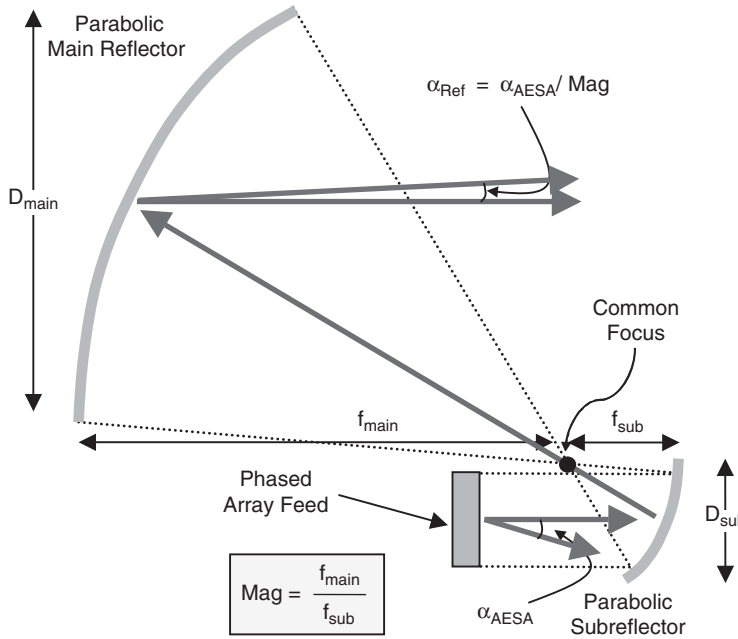

FIGURE 12.24 Confocal dual reflector antenna

Scan aberrations lead to moderately higher scan losses and slight beam scan angle deviations from those predicted by Eqs. 12.29 and 12.30 when ideal ESA plane wave excitations, i.e., linear phase slope, are applied. However, the amplitude and phase controls in the ESA allow for scan aberration compensation via conjugate matching of the aperture fields.[29] Thus, the use of an ESA feed enables recovery of scan losses resulting from aberrations in the system.

Confocal reflector architectures have been the subject of study and analysis for many years and numerous demonstration systems have also been developed.[25–28] Although confocal reflectors have not been adopted for significant usage in operational systems, these reflector systems are likely to be part of some next-generation radars due to the relatively recent maturation of enabling ESA technology.

Spherical Reflectors.[31–34] The spherical reflector[31] is sometimes used for applications requiring scanning or multiple beams over very wide angles. Its design is based upon the fact that, over limited angular regions, a spherical surface viewed from any point halfway between the center of a sphere and its surface is nearly parabolic. This means that if a feed is moved along an inner spherical surface of constant radius $R/2$, where R is the radius of the spherical reflector, the secondary beam can be steered. The range of beam steering is limited by the size of the spherical reflector, i.e., the portion of a full sphere realized by the reflector. The scanning capability can be implemented via use of either a single movable feed or an array with switchable feeds.

Self-blockage (reflector blocking itself) is another potential limiting factor in spherical reflector systems. However, 360° of azimuth steering can be accomplished via a polarization design scheme similar to the polarization twist subreflector described

above[24] for the Cassegrain system. In this design, the feed polarization is tilted 45° and the reflector is formed of conducting strips parallel to the polarization. However, the conducting strips on opposing sides of the reflector are twisted 90°, thereby enabling transmission of the reflected energy. This type of antenna is known as a *helisphere*.

If wide angle scanning in only one plane, i.e., azimuth or elevation, is required, a similar design called the *parabolic torus*[32] is more applicable. The parabolic torus reflector is a surface that is spherical in one plane (azimuth or elevation) and parabolic in the other plane. This design takes advantage of both the wide scanning enabled by the spherical shaping and the high aperture efficiency enabled by the parabolic shaping. The height (elevation) dimension of the reflector is set by the required elevation beamwidth.

The parabolic torus has seen application in various radars including the original BMEWS system[33] and the SPS-30 and SPQ-9B[34] systems.

12.4 REFLECTOR FEEDS

Whereas phased array antennas are frequently chosen for radar system designs, reflector antennas were once the dominant antenna design choice for medium- to high-gain radar apertures. Obviously, the cost of a single feed horn and metal reflector is much less than the same size array with many individual elements and associated phase shifters, amplifiers, receivers, etc. Consequently, many radars currently in the field use reflector antennas. Furthermore, reflector antenna designs are used in modern radar designs where moderate scan rates and scan volumes are required or low cost is essential.

Many legacy radars employ reflector antennas with single feed elements or a cluster of feeds (i.e., an array) with a fixed beam RF combiner or divider network. Figure 12.25 shows some typical single-feed reflector configurations utilizing horn, waveguide, and dipole feeds. Figure 12.26 shows a few common types of flared horn feeds.

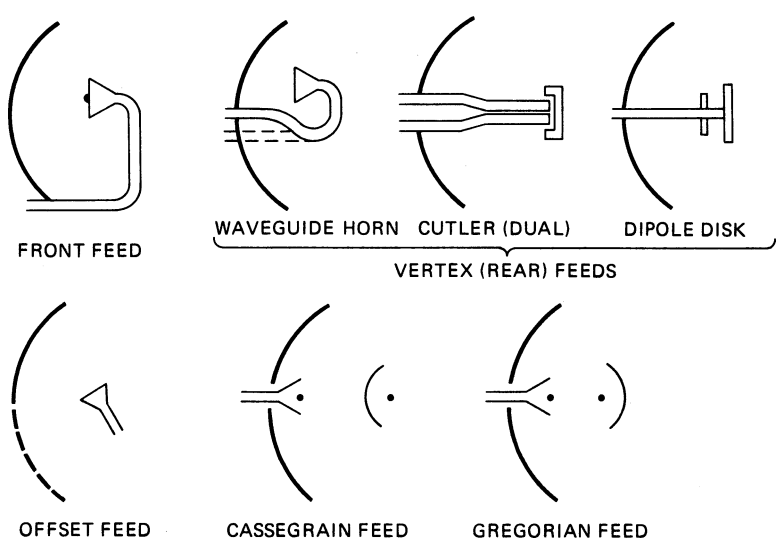

FIGURE 12.25 Some typical reflector antenna configurations

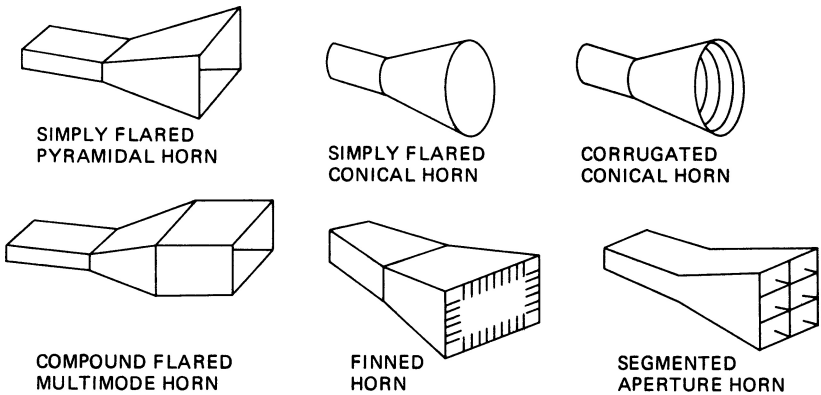

FIGURE 12.26 Various types of horn feeds for reflector antennas

Other types of feeds such as dipoles, microstrip patches, notches, etc., are sometimes used, but for single-feed reflector implementations, flared waveguide horns are the most common. The feed (in conjunction with the reflector) must also satisfy the antenna polarization requirements and handle required peak and average power levels under all operational environments. Other feed design considerations include the operating bandwidth and the potential implementation of any additional modes/patterns, e.g., difference or squinted beams.

For single-feed radar reflector antennas such as those depicted in Figures 12.25, mechanical scanning is generally achieved via a gimbal (a precision mechanical pointing system). Radar antenna gimbal designs vary greatly depending upon scan rate, FOV, tracking requirements, antenna size, mass, etc.

Basic Feeds.[35,36] For radars requiring a simple pencil beam, basic single mode waveguide horn feeds such as pyramidal (TE_{01} mode) and conical (TE_{11} mode) horns are widely used. Single-mode, flared horns will provide linearly polarized pencil beams and will generally handle high power. For more demanding applications requiring tracking modes, polarization diversity, high beam efficiency, or ultra-low sidelobes, feed designs become correspondingly more complex. For such applications, segmented, finned, multimode, and/or corrugated horns, as illustrated in Figure 12.26, are often used. Multimode feeds enable realization of difference mode patterns with a compact, single feed-horn and, as such, are especially useful for tracking applications.

Monopulse Feeds.[37–40] Monopulse is frequently used in radar tracking and surveillance systems to either keep the beam pointed on the target (tracking) or to accurately measure the angle to the target (surveillance).[37–40]

Amplitude comparison monopulse systems, illustrated in Figure 12.27, use the sum of the two feed

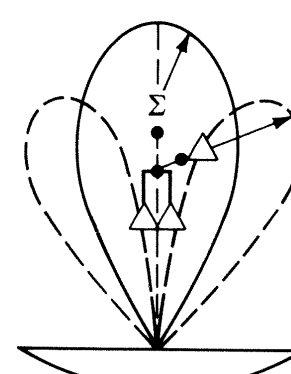

FIGURE 12.27 Amplitude comparison monopulse antenna showing sum and difference beams

outputs to form a high-gain low-sidelobe beam and the difference of the two squinted beams to form a precise, deep null at boresight. The sum beam is used on both transmit and receive to detect the target. The difference beam is receive only and provides angle determination. In most applications, both azimuth and elevation difference beam ports are implemented. Figure 12.27 illustrates the concept of amplitude comparison monopulse. A feedback loop minimizes the received difference beam signal by mechanically steering the antenna to keep the null (and the corresponding sum beam peak) on target.

There are numerous ways to realize amplitude monopulse beams in a reflector antenna design, but most designs generally fall into two classes; (1) multifeed and (2) multimode. Multifeed designs use combining networks to generate differential feed distributions. In its simplest form, an (az/el) multifeed monopulse feed array can be realized as a four-element feed, as shown in Figure 12.28. However, some applications use more feed elements to further tailor the distribution to improve efficiency and/or difference beam slope.

If the reflector is illuminated with a simple four-element feed, a conflict generally arises between the goals of high sum-beam efficiency and high difference-beam slope from the monopulse comparator. The former requires a small overall feed size, whereas the latter requires large individual feeds (Figure 12.29). Numerous design methods have been devised to overcome this problem, as well as the associated high difference pattern sidelobes. These methods either use different sets of feed elements for the sum and difference beams or apply different array amplitude/phase weightings for each of the beams. If horn feed elements are used, one approach is to oversize the feeds to enable multimode excitation for the sum beam as described by Hannan.[40] A comparison of some common monopulse feed configurations is included in Table 12.2.

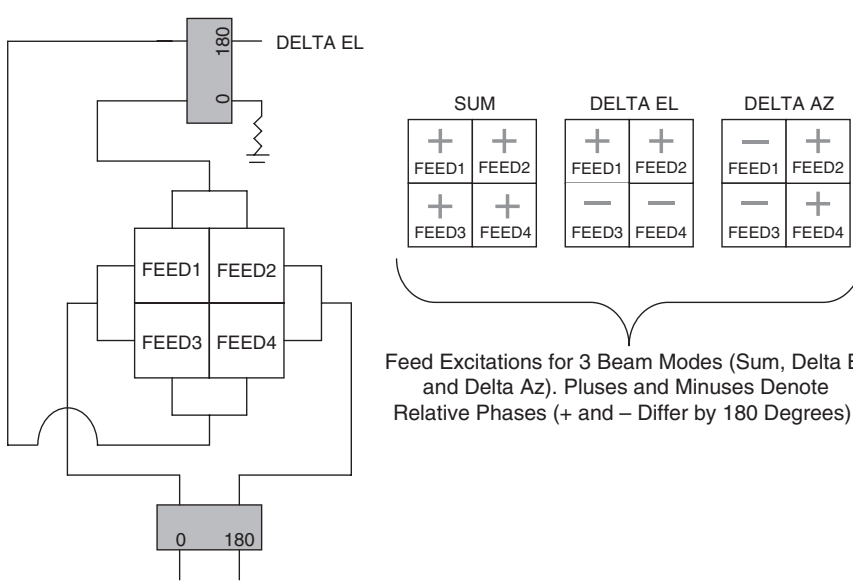

FIGURE 12.28 Four-element monopulse feed with dum, delta az, and delta el ports

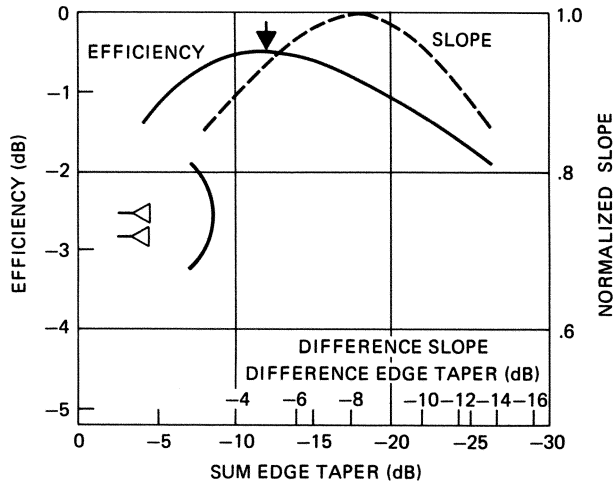

FIGURE 12.29 Plots of sum-beam efficiency and difference-beam slope as a function of associated edge tapers (*H*-plane shown)

Array Feeds. A single feed at the focal point of a parabola forms a beam parallel to the focal axis. Additional feeds displaced from the focal point form additional beams at angles from the axis (see Eq. 12.21). Thus, one can employ a multiple feed array with appropriate electronics to feed a reflector and provide either multiple displaced beams or electronic beam switching, i.e., beam scanning to discrete angles. A reflector system such as this can effectively provide electronic scanning over a narrow FOV. However, this type of array-fed reflector architecture does suffer from one drawback. A parabola converts a spherical wave into a pure plane wave only when the source (feed) is at the focus. If the source (feed) is displaced from the focus, the reflected wave is somewhat distorted and this results in gain loss and beam shape distortion. Figure 12.30 shows the effect of this distortion on the pattern of a typical center-fed reflector as the feed is moved off-axis.

TABLE 12.2 Monopulse Feedhorn Performance

	H plane		*E* plane	Sidelobes, dB		
Type of Horn	Efficiency	Slope	Slope	Sum	Difference	Feed shape
Simple four-horn	0.58	1.2	1.2	19	10	
Two-horn dual-mode	0.75	1.6	1.2	19	10	
Two-horn triple-mode	0.75	1.6	1.2	19	10	
Twelve-horn	0.56	1.7	1.6	19	19	
Four-horn triple-mode	0.75	1.6	1.6	19	19	

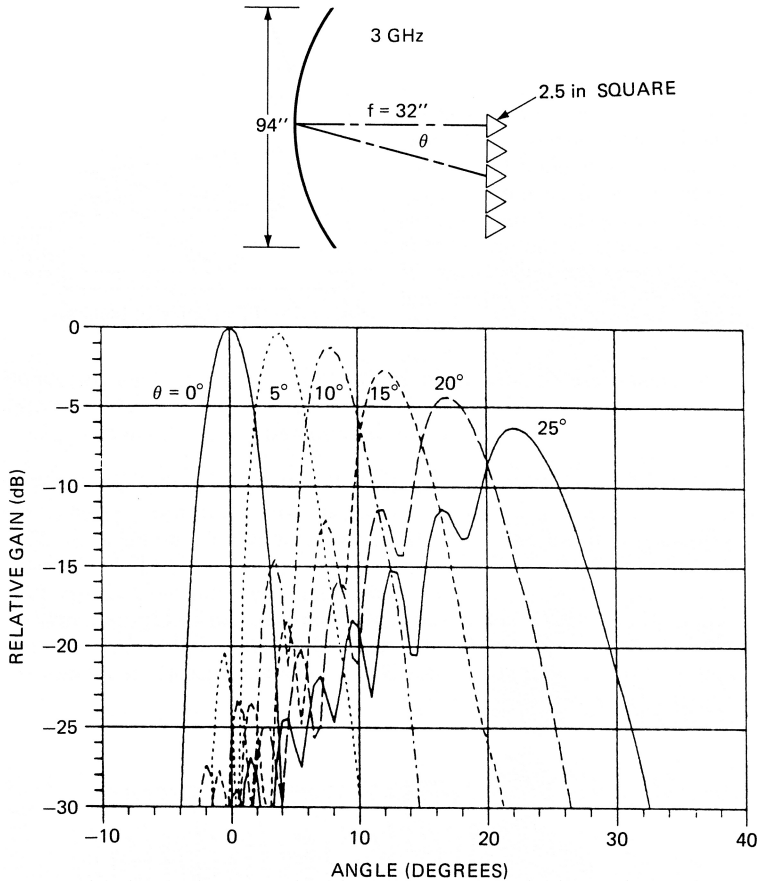

FIGURE 12.30 Patterns for off-axis feeds

A phased array (ESA) type feed covering the focal region (planar or curved in shape), such as that shown in Figure 12.31*b*, can provide improved capability. It offers two enhancements that extend the capability above and beyond that of a multiple feed array with switched beams. The phased array fed reflector can transmit or receive beams over continuous angles within the FOV whereas the multiple feed array is limited to discrete beam positions. It also provides greater aperture efficiency because it allows for adjustment of the element amplitudes and phases to reduce scan losses due to aberrations. If we view the reflector as a collector of parallel rays from a range of angles covering the FOV and examine the converging ray paths (Figure 12.31*a*), it is evident that an appropriately sized feed region can be found that intercepts most of the energy. If the phased-array feed array is appropriately designed, beam distortion and scan losses (such as those shown in Figure 12.30) can be effectively eliminated. This sort of design approach wherein the feed array amplitude/phase distribution is "matched" to the focal plane fields is often referred to as *conjugate field matching*.[41]

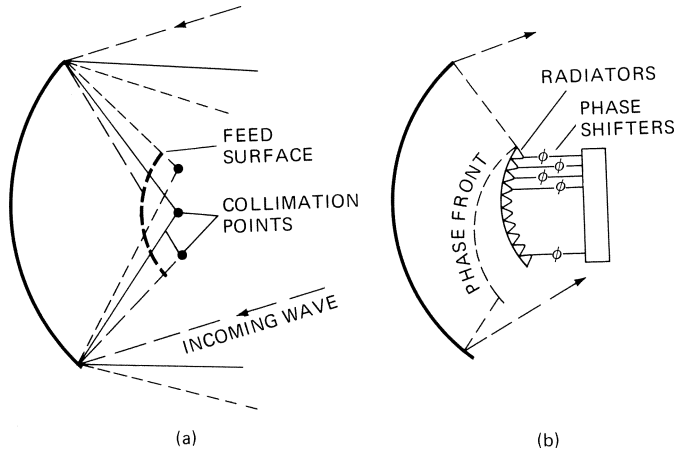

FIGURE 12.31 Extended feed region improves sidelobes of offset feed (used on ARSR-4): (*a*) ray geometry and (*b*) curved feed

Feed arrays, such as that illustrated in the ARSR-4 reflector antenna shown in Figures 12.31 and 12.32, have also been used to enable shaped beams and low sidelobe patterns. Passive combiner networks are used to generate multiple receive beams stacked in elevation and a single transmit beam. The receive beams require low azimuth sidelobes. A conventional beamforming approach would incorporate an array at the focal plane with a single beam per feed; however, the associated phase distortion due to displacement causes poor azimuth sidelobes. To correct this problem, the feed array is placed forward of the azimuth focal point, enabling compensation and sidelobe improvements via use of multiple feeds per beam with appropriate feed phasing (Figure 12.31*a*). Two different focal lengths are used in the reflector, one for elevation and a longer one for azimuth. The feed is on a curved surface, optimized via ray tracing, and is forward of the azimuth focal point. For each row, the amplitude and phase is optimized for a beam with low azimuth sidelobes. The elevation patterns for each single row have poor sidelobes, but several rows are used for each receive beam thereby improving the elevation sidelobes. For transmit, all 24 rows (the whole array) are used. On receive, 9 groups of rows are used to form 9 receive beams.

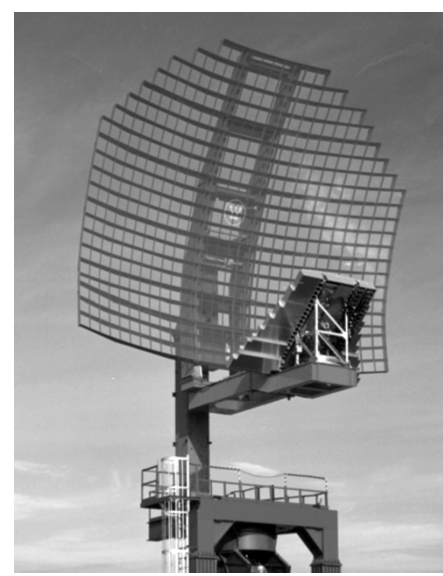

FIGURE 12.32 ARSR-4 low-sidelobe reflector with offset array feed (*Courtesy Northrop Grumman Corporation*)

12.5 REFLECTOR ANTENNA ANALYSIS

Reflector antenna analysis methods can generally be lumped into three classes or categories: (1) Physical Optics (PO), or induced current methods, (2) Geometrical Optics (GO) methods, with and without diffraction terms, and (3) rigorous, or full-wave, methods.

Physical Optics (PO) Reflector Analysis. The Physical Optics (PO) method is commonly employed for the most rigorous reflector analysis due to its accuracy. It incorporates the field properties of the feed, and models the resultant fields from the reflector, thus enabling the computation of the cross polarization properties. Furthermore, the method is more accurate for feeds that are not at the focal point and reflectors that are not parabolic. There are many good references that describe the theory behind the method and how it is applied to the analysis of reflector antennas.[42–44] PO is a very general "high frequency" analysis method that generally provides high fidelity pattern predictions for most reflector systems as long as the reflector dimensions are large, say, greater than about five wavelengths in both dimensions. An overview of PO is provided here to enable an understanding of the fundamentals of the method. The PO method can be broken into two steps: (1) the calculation of induced reflector surface currents, and (2) the integration of these currents (with an appropriate free space vector Green's function kernel) to determine the far-field patterns.

First, consider the calculation of the reflector surface currents. It is assumed that the field from the feed that is incident on the reflector has a spherical wavefront with amplitude tapering defined by the feed pattern. So, as a first step, the feed is mathematically modeled to determine the incident field amplitude and phase at the reflector surface. Different models are applied depending on the choice of feed used in the design; examples include waveguide feed horns, microstrip patches, dipoles, etc. Sometimes the feed model will instead employ measured feed patterns if such data is available. All models must be normalized to some prescribed radiated power level, e.g., 1 watt. Figure 12.33 shows a typical waveguide feed horn model and its associated local coordinate system.

Based on an appropriate application of equivalence principle and the induction theorem,[42–44] the currents induced on the reflector can be determined from the feed

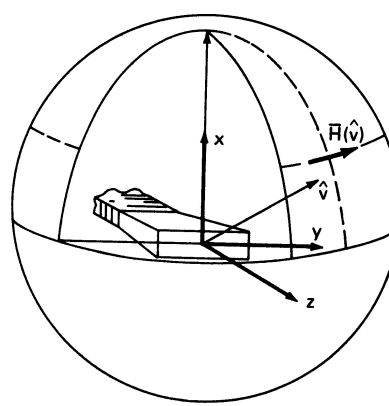

FIGURE 12.33 Waveguide feed horn model and coordinate system

$\bar{H}$-field incident at the surface of the reflector. The key premise of the equivalence principle is that fields from a scatterer (e.g., a reflector) can be represented by an "equivalent" electric current $\bar{J}$ and magnetic current $\bar{M}$ that are directly related to the incident $\bar{E}$ and $\bar{H}$ fields via

$$\bar{J} = \hat{n} \times \bar{H} \tag{12.31}$$

$$\bar{M} = -\hat{n} \times \bar{E} \tag{12.32}$$

where $\hat{n}$ is the normal to the reflector surface. The application of the equivalence principle to PO-based reflector analyses as shown here is a specialized case wherein the reflector is an electric conductor, and contributions from surface currents on the backside of the reflector are deemed negligible. An appropriate application of image theory[42–44] imposes a zero tangential E-field (Eq. 12.32) and doubles the electric current, $\bar{J}$ (Eq. 12.31), resulting in an equivalent surface current represented by

$$\bar{J} = 2\hat{n} \times \bar{H} \tag{12.33}$$

Now consider a generalized reflector surface as shown in Figure 12.34. The surface is divided into rectangular grid regions of area dA that intercept the incident feed field. If the feed far-field H-field pattern is $\bar{H}(\hat{v})$, polarized in the direction $\hat{v}$, then the incident H-field at the reflector is

$$\bar{H} = \bar{H}(\hat{v})\,(\hat{v} \cdot \hat{n})\, e^{-jkr} dA/4\pi r \tag{12.34}$$

Combining Eqs. 12.34 and 12.33 yields the equivalent surface current $\bar{J}$ at area dA

$$\bar{J} = 2\hat{n} \times \bar{H}(\hat{v})\,(\hat{v} \cdot \hat{n})\, e^{-jkr} dA/4\pi r \tag{12.35}$$

where $\hat{n}$ is the normal to the surface, $\hat{s}$ is the observation direction (Figure 12.34), r is the distance from the feed to the reflecting surface, $k = 2\pi/\lambda$, i.e., the wavenumber, and the $e^{-jkr}/4\pi r$ term accounts for the propagation phase and space loss from the feed to the reflector surface.

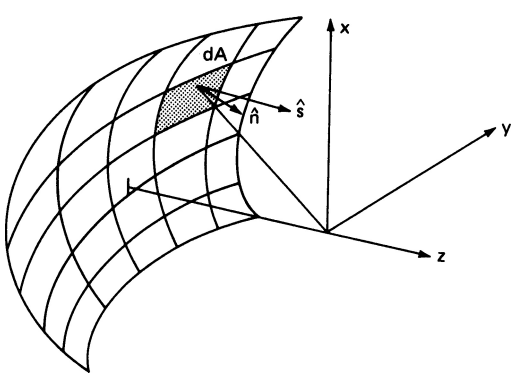

FIGURE 12.34 Generalized reflector geometry

The final step in the PO-based pattern solution is to calculate the reflector far fields via a vector integration of the product of the surface current and the free space Green's function.[44] The magnetic vector potential $\bar{A}$ is defined by the equation

$$\bar{A} = \iiint \frac{\bar{J}\, e^{-jk|r-r'|} dr'}{4\pi\, |r-r'|} \tag{12.36}$$

The vector $\bar{E}$-and $\bar{H}$-fields are related to $\bar{A}$ via simple derivatives and/or vector multiplications. In practice, Eq. 12.36 is computed as a summation of numerical integrations. Proper convergence of the field solution and resulting patterns is a function of the grid size, and this is generally achieved and verified by incrementally decreasing the grid size until the solution stabilizes. Achieving sufficient convergence in reflector PO computations within reasonable computer run times (a few minutes or less) is rarely a problem with modern computers.

Geometrical Optics (GO) Reflector Analysis, Including GTD/UTD. There are a variety of GO-based pattern reflector analysis methods, all of which are rooted in ray tracing and some of which are augmented with diffraction terms for improved accuracy. Although the simple GO method (no diffraction terms) works reasonably well, it is not generally as accurate as PO. However, two of the more common enhanced methods, Geometrical Theory of Diffraction (GTD) and Uniform Theory of Diffraction (UTD),[45] include edge diffraction and are much more accurate. UTD is essentially an enhancement of GTD wherein localized GTD singularities are corrected. The diffraction terms in UTD increase the accuracy of the basic GO solution and will properly predict the pattern asymmetries of more generalized reflector geometries. Like PO, GTD/UTD methods will generally provide high-fidelity pattern predictions for most reflector systems (center-fed, offset, single, dual, etc.) as long as the reflector size is approximately 5λ or larger. More detailed descriptions of GTD/UTD can be found in various references.[45,46]

Full-Wave Reflector Analysis Methods. Rigorous or full-wave methods include, for example, the method of moments (MOM), the finite element method (FEM), and the finite difference time domain (FDTD) method. Although these methods are very rigorous and highly accurate, they are not generally employed for reflector design/analysis because they tend to be too computationally intensive. These methods are more typically applied for precision analysis of microwave devices or electrically "smaller" antennas, e.g., radiators and feeds, that are no more than a few wavelengths in size. In recent years, hybrid methods incorporating PO or GO/GTD along with MOM, FEM, or FDTD have been developed. These methods enable enhanced reflector feed modeling, i.e., integrated with reflector analysis, and rigorous modeling of electrically small scatterers, e.g., small subreflectors or feed support struts.

Computer Codes for Reflector Design and Analysis. A number of commercial and university codes have been developed for the analysis and design of reflector systems. Two of the more well-known and commonly used codes are GRASP and the SATCOM Workbench with its NEC-REF module. GRASP is a commercially available PO-based reflector design and scattering analysis code developed by TICRA (Copenhagen, Denmark). The SATCOM Workbench was developed by The Ohio State University ElectroScience Laboratory (OSU-ESL) and is a user-friendly code that incorporates a wide variety of software modules, some of which are based upon legacy

OSU codes such as NEC-REF (OSU Reflector Code). The SATCOM Workbench is available to members of the USA Satellite Industry Code Consortium.[47]

TICRA GRASP is a generalized PO-based code intended for both reflector system design/analysis and scattering analyses. GRASP has popular GUI-versions that run on Microsoft PC-based Windows operating systems (2000, 2003, NT, XP) as well as LINUX. Although the GRASP code is PO-based, it also includes a Physical Theory of Diffraction (PTD) option as well as a Geometrical Optics (GO)/ Uniform Geometrical Theory of Diffraction (UGTD) option that can be turned on when needed. The code is very general in that it can model standard conic section-based reflectors as well as arbitrarily shaped surfaces or scatterers if desired. It also has a suite of feed models to draw upon and has tools to enable feed array modeling. Figure 12.35 shows a snapshot of the GRASP GUI window, including a rendering of an array-fed reflector and its associated beam rosetta, i.e., an overlay of beams associated with each of the individual array feeds. Some other notable features of the GRASP code include scattering models for mesh, frequency selective or lossy reflector surfaces, and a spherical wave expansion (SWE) feature for modeling of systems wherein the reflector or scatterer is in the near field of the feed source. Finally, there are various other antenna software modules available from TICRA that can be used in conjunction with GRASP. One notable example is Physical Optics Shaper (POS), an optimizer module for shaped reflector synthesis and/or feed array amplitude/phase weight synthesis. More information is available at www.ticra.com.

The OSU-ESL SATCOM Workbench[47] is a Microsoft Windows–based modular software package for PC platforms running Windows 95/98/2000/XP. It contains a variety of modules or so-called wizards in addition to the generalized GO/GTD-based reflector/scattering code backbone. The core GO/GTD reflector/scattering

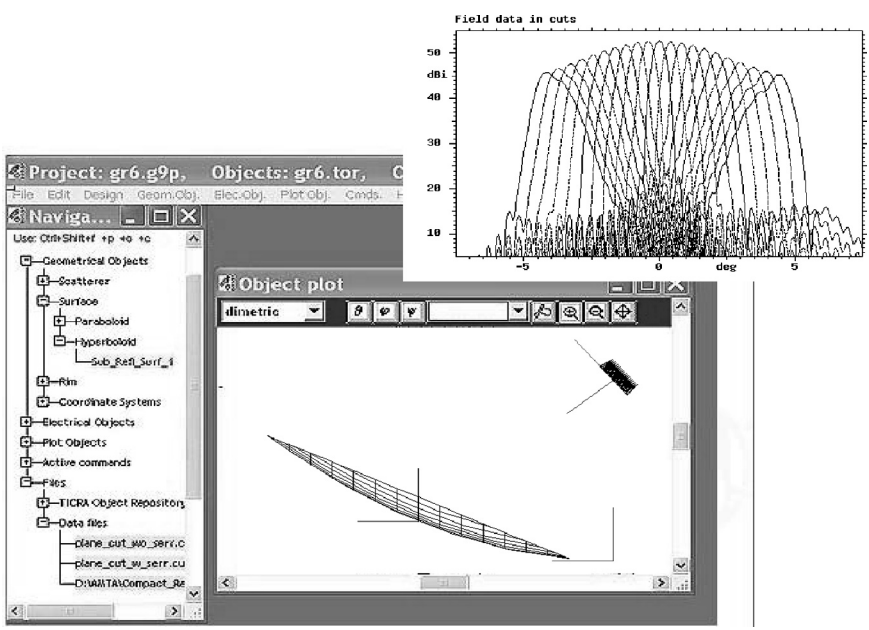

FIGURE 12.35 TICRA GRASP GUI, multibeam array-fed reflector model and patterns

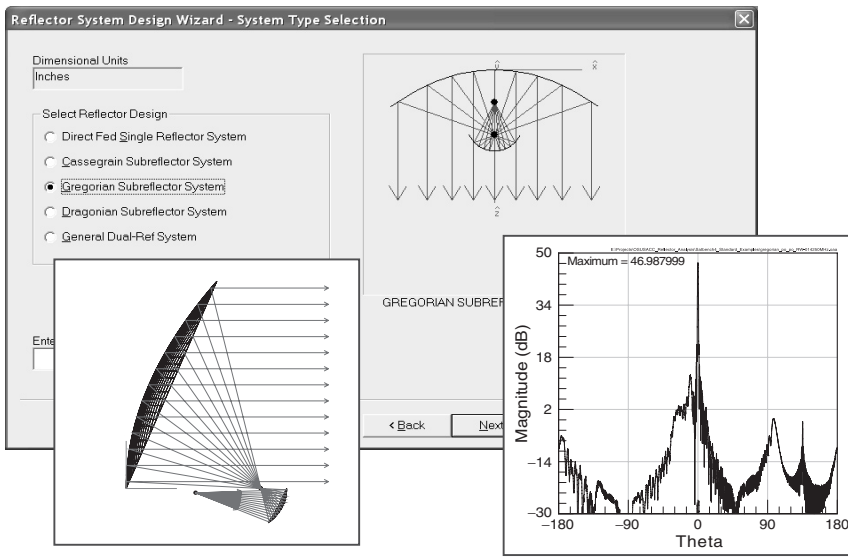

FIGURE 12.36 OSU-ESL SATCOM Workbench GUI, offset Gregorian reflector model and pattern

code portion of the SATCOM Workbench is based upon the legacy NEC-REF and NEC-BSC codes. The EM Workbench, like GRASP, is very general in its capabilities, i.e., it can handle a diversity of reflector/scatterer shapes and combinations and also has various feed models to draw upon. It also has feed and array wizards that employ full-wave EM models that can be used as sources for reflector and scattering design/analyses. Figure 12.36 shows a snapshot of the Workbench GUI window, including a rendering of an offset-fed reflector and its associated beam pattern. More information is available at esl.eng.ohio-state.edu.

12.6 MECHANICAL DESIGN CONSIDERATIONS

Reflector mechanical design is a detailed discipline unto itself with a multitude of factors to consider. Furthermore, designs vary significantly depending upon many factors, including platform, reflector size, environment, frequency of operation, scan/FOV, and cost constraints. Although it is not within the scope of this chapter to address mechanical design in detail, a brief survey of design factors and considerations provides some useful insights.

The platform, i.e., vehicle, or installation site is a significant driver for radar sensors in general, including the antenna. *Platform* is a generic term referring to the vehicle where the radar and antenna are installed. Typical radar platforms include pedestal (fixed site), ground vehicles, ships, airplanes, UAVs, and spacecraft/satellites. The following short section is devoted to platform impacts and some key associated design drivers. These include mass, volume (stowage/deployment), gimbals (precision mechanical positioning systems), materials, and mechanical tolerances. Finally, there is a brief discussion of environmental design considerations and radomes.

Installation Is a Significant Mechanical Design Driver. The platform is generally a dominant mechanical design driver because it determines the environment (thermal, vibration, etc.), and it typically drives the available size, weight, and power (SWAP) for the radar and the reflector antenna. Table 12.3 provides a qualitative comparison of typical design requirements and features for radar reflector antennas on ground-based, ship-based, airborne, and spaceborne platforms.

Mass, Volume, Stowage, Deployment, and Gimbaling. The degree to which these five factors, *mass, volume, stowage, deployment*, and *gimbaling* drive the reflector design vary in accordance with the reflector system and the platform. However,

TABLE 12.3 Mechanical Design Drivers for Reflector Antenna Systems as a Function of Platform

PLATFORM DRIVES REFLECTOR ANTENNA MECHANICAL DESIGN				
	Ground-based	Ship-based	Airborne	Spaceborne
Mass	• Typically not a major driver. • May be a driver if field deployment is required.	• Typically not a major driver.	• Typically a significant driver. • Could be a major driver depending on size of antenna and platform.	• A major driver; launch costs are very high and are driven by available volume and mass for radar payload. • Use of light weight materials is important.
Volume	• Typically not a major driver. • May be a driver if field deployment is required	• Depends, a driver in some cases	• Typically a significant driver • Could be a major driver depending on size of antenna and platform	• A major driver; launch costs are very high and are driven by available volume and mass for radar payload. • Once in space, antenna deployments are typically needed, e.g., unfolding, etc.
Thermal	• Can be a major driver. • Radars are typically high power. • High power densities at feed or feed array are common. • Cooling system design to maintain feed temp can be a challenge.	• Can be a major driver. • Radars are typically high power. • High power densities at feed or feed array are common. • Cooling system design to maintain feed temp can be a challenge.	• Can be a major driver. • Radars are typically high power. • High power densities at feed or feed array are common. • Cooling system design to maintain feed temp can be a challenge.	• A major driver, need sophisticated modeling to predict solar heating throughout orbit. • Passive cooling systems are generally employed, e.g., heat pipes.
Vibration	• Typically not a major driver. • However, must consider vibration during transport (truck, airplane, other?).	• Typically not a major driver.	• Typically a major driver.	• Typically a major driver, driven by launch vehicle (rocket).

TABLE 12.3 Mechanical Design Drivers for Reflector Antenna Systems as a Function of Platform (*Continued*)

PLATFORM DRIVES REFLECTOR ANTENNA MECHANICAL DESIGN				
	Ground-based	Ship-based	Airborne	Spaceborne
Stowage/ Deployment	• Can be a driver if system is transportable.	• Typically not a requirement.	• Typically not a requirement, but there are exceptions.	• Typically required, generally a major design driver. • Reliability of deployment is a major concern; mission depends on it.
Other	• Is transportability a requirement? Are there multiple environments to which the radar antenna will be exposed?	• Where on the ship is the radar antenna? Is it covered with a radome? Will it be exposed to water or wave slap?	• Volume is a major constraint, not much room for antenna apertures.	• Specialized environments. • Launch drives vibration and acoustic loads. • Radiation a driver at some orbits. • Thermal extremes, including gradients, are a concern.

mass and volume constraints generally have a significant impact on the reflector system design. Furthermore, some sort of stowage and deployment of the reflector is sometimes required, especially for larger reflectors. These considerations and constraints drive the choices of materials, structural designs, passive and active mechanisms, etc. It is beyond the scope of this chapter to address this topic in detail. However, it's useful to show a couple examples for illustration.

Consider, first, a ground-based dual-reflector design with a 9-meter main reflector aperture. This reflector, shown in Figure 12.37, is used for an S-band meteorological radar application.[48] The panelized aluminum reflector is mechanically scanned via use of a gimbal (not shown). The feed, a dual-polarized waveguide horn, is also shown in Figure 12.37. The structural design of this large reflector was a significant task driven by the need to maintain low reflector surface distortion (less than 50 mils) with severe wind and gravity-loading forces and thermal gradients.

The second example is a space-based deployable reflector. The mesh reflector, shown in both stowed and deployed configurations in Figure 12.38, is an offset reflector with a 12.25 meter circular projected aperture.[49] This L-band design, developed by Northrop-Grumman Space Technologies Astro Aerospace group, has been successfully launched and deployed and is currently in use on several communication satellites.[50] A total of five reflectors of aperture diameters 9 meters, 12 meters, and 12.25 meters have been flown. Studies have addressed the potential usage of this reflector technology for various space-based radar applications, including weather sensing/monitoring (NEXRAD)[51] and planetary SAR mapping missions (lunar and Mars). Significant features of this reflector include its precise surface accuracy, high stiffness and stability, low mass, and reliable deployment. For example, for the reflector shown in Figure 12.38, an RMS surface accuracy of less than 50 mils from all error sources including in-orbit thermal gradients was achieved via prudent material choices and matching of the associated material coefficients of thermal expansion (CTEs). Pointing precision due to eclipse thermal snap has been measured in orbit at less than 0.01 degrees.[52]

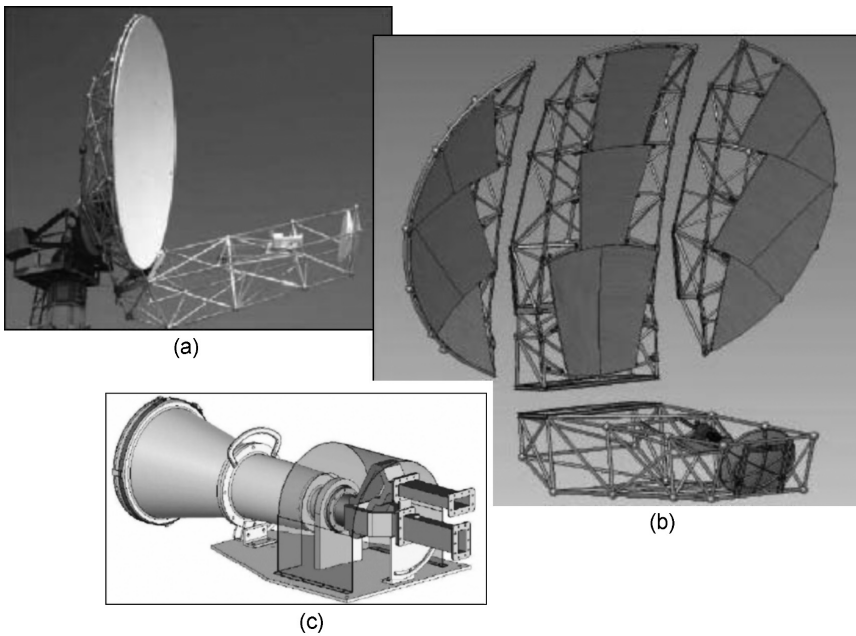

FIGURE 12.37 Ground-based S-band 9-meter dual reflector and dual-pol feed: *a*) photo of system; *b*) mechanical CAD rendering showing panelized reflector surface and support structure; and *c*) dual-polarized waveguide feedhorn (*Courtesy General Dynamics C4 Systems*)

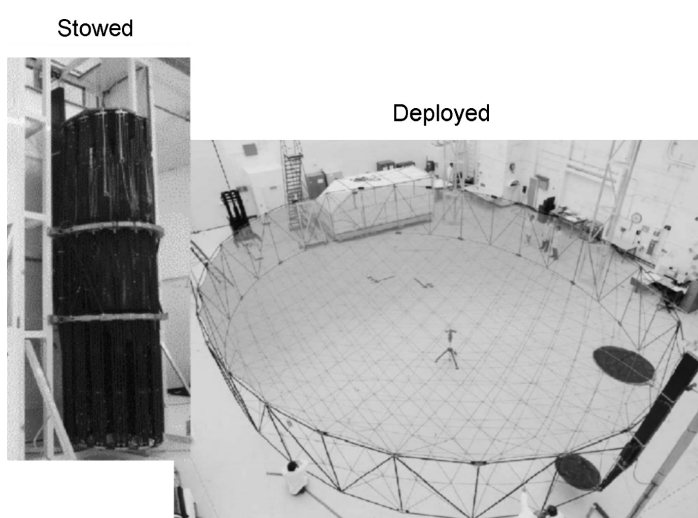

FIGURE 12.38 Space-based deployable L-band ASTROMesh reflector with 12.25 meter circular projected aperture (*Courtesy Northrop Grumman Corporation*)

Deployable space-based reflectors have also been developed by the Harris Corporation for various space-based communications applications. See www.harris.com for more details.

Because most reflector designs have at best limited electronic scan capability, a gimbal is typically needed to extend the (mechanical) FOV for the radar. The key factors or specifications that typically drive the design or procurement of the gimbal are scan rate, slew requirements, acceleration/deceleration requirements, torque and load (reflector mass) requirements, power requirements, etc. It is important for the radar system engineer to understand these factors and associated practical gimbal design limits.

Environmental Factors and Considerations. The impact of environmental factors varies widely, but some of the factors that are typically significant include thermal, vibration, and exposure (e.g., salt, sand, water, radiation, etc.). Thermal effects, i.e., spatial or temporal temperature variations, are of particular concern for spaceborne sensors that often see very significant temperature changes (greater than 100° C temporal or spatial variation is not uncommon). Vibration is another concern, especially for airborne and spaceborne reflectors. Reflectors on these platforms generally see particularly stressing vibration levels driven by airplane or launch vehicle (rocket) environments. Potential exposure to salt, sand, water, etc., is highly dependent upon platform, use of radome (or not), etc., but must be considered in the design.

Radomes. Radomes are used when it is necessary to protect antennas from adverse environmental effects. Ideally, a radome should be perfectly transparent to the RF radiation from (or to) the antenna and yet be able to withstand such environmental effects as wind, rain, hail, snow, ice, sand, salt spray, lightning, and (in the case of high-speed airborne applications) thermal, erosion, and other aerodynamic effects. In practice, these environmental factors determine the mechanical design of the radome, and the desire for ideal RF transparency must be compromised because mechanical and electrical requirements are often in conflict.

Radomes cause four major electrical effects on antenna performance. *Beam deflection* is the shift of the electrical axis, which is critical for tracking radar. *Transmission loss* is the measure of energy lost by reflection and absorption. The *reflected power* causes antenna mismatch in small radomes and sidelobes in larger radomes.

Radome design is a specialized art, and many books[53,54] are devoted to its intricate details. This section makes no attempt to provide radome design information as such but instead is aimed at making the radar system designer aware of the basic concepts behind the types of radomes available for various applications.

Three general classes of radome are of interest for reflector antenna applications: *feed covers*, which often have to endure pressure, high voltage, and heating; *covers attached to the reflector*, which alter the pattern in a fixed manner; and *external radomes*, within which the antenna moves. External radomes are the most common and will, therefore, be emphasized. Within each class, a variety of skin and skin-supporting designs is available to minimize the electrical effects under the constraints of the environment. The radome skin may be rigid, supported by a framework, or air-supported.

The most common rigid radome-wall structures are shown in Figure 12.39 and are known as homogeneous single layer, A-sandwich, B-sandwich, C-sandwich, multiple-layer sandwich, and dielectrics with metal inclusions.

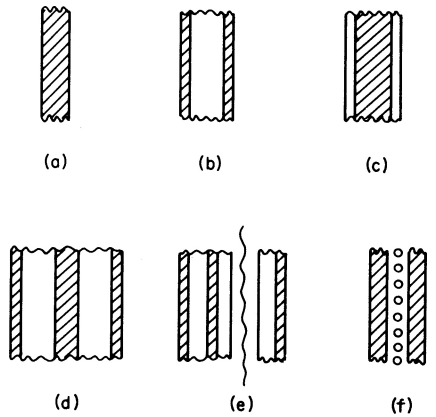

FIGURE 12.39[54] Common radome-wall cross sections: (*a*) single layer, (*b*) A-sandwich, (*c*) B-sandwich, (*d*) C-sandwich, (*e*) multiple-layer sandwich, and (*f*) dielectrics with metal inclusions

Single Layer. The homogeneous single-layer radome has been used in many radome applications. Materials for this type have included fiberglass-reinforced plastics, ceramics, elastomers, and monolithic foam. The optimum thickness for a single layer is a multiple of a half wavelength in the dielectric material at the appropriate incidence angle, but many single-layer radomes are simply thin-wall approximations to the zero-thickness case.

A-Sandwich. A commonly used radome-wall cross section is the A-sandwich, which consists of two relatively dense thin skins and a thicker low-density core. This configuration exhibits high strength-to-weight ratios. The skins are generally fiberglass-reinforced plastics, and the core is a foam or honeycomb. Inorganic skin and core sandwiches also have been developed for high-temperature applications. As a rule, the skins of the sandwich are made symmetrical or of equal thickness to allow midband cancellation of reflections.

B-Sandwich. In contrast to the A-sandwich, the B-sandwich is a three-layer configuration whose skins have a dielectric constant lower than that of the core material. This wall cross section is heavier than that of the A-sandwich because of the relatively dense core. The B-sandwich is not commonly used because the core dielectric constant is quite high for a proper match.

C-Sandwich. The C-sandwich is a five-layer design consisting of outer skins, a center skin, and two intermediate cores. The symmetrical C-sandwich can be thought of as two back-to-back A-sandwiches. This configuration is used when the ordinary A-sandwich will not provide sufficient strength, or for certain electrical performance characteristics, or when one layer is to serve as a warm-air duct for deicing.

Multiple-Layer Sandwich. Multiple-layer sandwiches of 7, 9, 11, or more layers are sometimes considered when great strength, good electrical performance, and lightweight are required. Some of these designs have used thin layers of fiberglass

laminates and low-density cores to attain high transmission performance over large frequency bands.

Dielectric Layers with Metal Inclusions. Metal inclusions have been considered for use with dielectric layers to achieve frequency filtering, broad-frequency-band performance, or reduced-thickness radomes. Thin layers of metal inclusions exhibit the characteristics of lumped circuit elements shunted across a transmission line. For example, a grid of parallel metal wires exhibits the properties of a shunt-inductive susceptance.

There are many additional radome design issues and application specific considerations and design drivers, but these are beyond the scope of this chapter.

ACKNOWLEDGMENTS

The authors wish to acknowledge and thank Helmut Schrank, Gary Evans, and Daniel Davis (also co-author of this chapter) for Chapter 6, "Reflector Antennas," in the second (1990) edition of this handbook.[55] We are grateful for their contributions and portions of the second edition chapter have been retained.

Portions of the material in the "Radome" subsection were adapted from Chapter 14,"Radomes," in the first (1970) edition of this handbook,[56] which was authored by Vincent J. DiCaudo.

REFERENCES

1. J. D. Kraus, *Antennas*, 2nd Ed., New York: McGraw-Hill Book Company, 1988: Sec. 2-34.
2. W. L. Stutzman and G. A. Thiele, *Antenna Theory and Design*, Chapter 8, New York: John Wiley and Sons, 1981.
3. C. M. Knop, "On the front to back ratio of a parabolic dish antenna," *IEEE Trans. Antennas Propag*., vol 24, pp. 109–111, January 1976.
4. W. V. T. Rusch, "Scattering from a hyperboloidal reflector in a cassegrain feed system," *IEEE Trans*., vol. AP-11, pp. 414–421, July 1963.
5. C. L. Gray, "Estimating the effect of feed support member blocking on antenna gain and sidelobe level," *Microwave J*., pp. 88–91, March 1964.
6. *Microwave Engineers Handbook and Buyers Guide*, New York: Horizon House, 1964, p. 143.
7. W. W. Mumford, "Some technical aspects of microwave radiation hazards," *Proc. IRE*, pp. 427–447, February 1961.
8. J. Ruze, "The effect of aperture errors on the antenna radiation pattern," *Nuovo Cimento, Suppl*., vol. 9, no. 3, pp. 364–380, 1952.
9. J. Ruze, "Antenna tolerance theory—A review," *Proc. IEEE*, vol. 54, pp. 633–640, April 1966.
10. S. Silver (ed.), *Microwave Antenna Theory and Design*, MIT Radiation Laboratory Series, vol. 12, New York: McGraw-Hill Book Company, 1949.
11. Y. T. Lo, "On the Beam Deviation Factor of a Parabolic Reflector," *IRE Trans*., vol. AP-8, pp. 347–349, May 1960.
12. P. D. Potter, "Application of spherical wave theory to Cassegrainian-fed paraboloids," *IEEE Trans*., vol. AP-15, pp. 727–736, November 1967.
13. R. C. Johnson and H. Jasik (eds.), *Antenna Engineering Handbook*, 2nd Ed., New York: McGraw-Hill Book Company, 1984, pp. 32–11, 32–12.

14. Y. T. Lo and S. W. Lee (eds.), *Antenna Handbook: Theory, Applications and Design, Reflector Antennas*, Chapter 15, New York: Van Nostrand Reinhold Co. Inc., 1988.
15. C. J. Sletten, "The theory of reflector antennas," Air Force Cambridge Res. Lab., AFCRL-66-761, Phys. Sci. Res., Paper 290, 1966.
16. K. S. Kelleher and H. P. Coleman, "Off-axis characteristics of the paraboloidal reflector," Naval Res. Lab. Rept. 4088, 1952.
17. A. W. Rudge and N. A. Adatia, "Offset parabolic reflector antennas: A review," *Proceedings IEEE*, vol. 66, no. 12, pp. 1592–1618, December 1978.
18. D. G. Kielsy, "Parabolic cylinder aerials," *Wireless Eng*., vol. 28, pp. 73–78, March 1951.
19. R. L. Fante et al., "A parabolic cylinder antenna with very low sidelobes," *IEEE Trans*., vol. AP-28, pp. 53–59, January 1980.
20. P. W. Hannan, "Microwave antennas derived from the cassegrain telescope," *IRE Trans*., vol. AP-9, pp. 140–153, March 1961.
21. P. D. Potter, "Aperture illumination and gain of a Cassegrainian system," *IEEE Trans*., vol. AP-11, pp. 373–375, May 1963.
22. W. V. T. Rusch, "Scattering from a hyperboloidal reflector in a Cassegrainian feed system," *IEEE Trans*., vol. AP-11, pp. 414–421, July 1963.
23. E. J. Wilkinson and A. J. Applebaum, "Cassegrain systems," *IRE Trans*., vol. AP-9, pp. 119–120, January 1961.
24. C. J. Sletten et al., "Offset dual reflector antennas for very low sidelobes," *Microwave J*., pp. 221–240, May 1986.
25. W. V. Rusch, "The current state of the reflector antenna art," *IEEE Trans. Antennas Propag*., vol. AP-32, no. 34, pp. 319–320, April 1984.
26. T. Haeger and J. J. Lee, "Comparisons between a shaped and nonshaped small cassegrain antenna," *IEEE Trans. Antennas Propag*., vol. 38, no. 12, December 1990.
27. R. A. Pearson, E. Elshirbini, and M. S. Smith, "Electronic beam scanning using an array-fed dual offset reflector antenna," *IEEE AP-S Int. Symp. Dig*., pp. 263–266, June 1986.
28. E. P. Ekelman and B. S. Lee, "An array-fed, dual-reflector antenna system (of offset confocal paraboloids) for satellite antenna applications," *IEEE Symp. Antennas Propag*., pp. 1586–1589, 1989.
29. H. K. Schuman and D. R. Pflug, "A phased array feed, dual offset reflector antenna for testing array compensation techniques," *IEEE Symp. Antennas Propag*., pp. 466–469, 1990.
30. W. D. Fitzgerald, "Limited electronic scanning with a near-field Cassegrainian system," Technical Report 484, MIT Lincoln Laboratory, 24 September 1971.
31. T. Lee, "A study of spherical reflectors as wide angle scanning antennas," *IEEE Trans. Antennas Propag*., vol. 7, pp. 223–226, July 1959.
32. T. Chu and P. P. Iannone, "Radiation properties of a parabolic torus reflector," *IEEE Trans. Antennas Propag*., vol. 37, no. 7, July 1989.
33. M. Skolnik, "A long range radar warning system for the detection of intercontinental ballistic missiles," MIT Lincoln Laboratory TR 128, August 15, 1956.
34. M. Skolnik, *Introduction to Radar Systems*, 3rd Ed., New York: McGraw-Hill, 2002, pp. 662, 663.
35. C. A. Balanis, *Antenna Theory Analysis and Design*, Chapters 13 and 15, New York: John Wiley and Sons, 1982.
36. A. W. Love (ed.), *Electromagnetic Horn Antennas*, New York: IEEE Press, 1976.
37. W. Cohen and C. M. Steinmetz, "Amplitude and phase sensing monopulse system parameters," *Microwave J*., pp. 27–33, October 1959.
38. D. R. Rhodes, *Introduction to Monopulse*, New York: McGraw-Hill Book Company, 1959.
39. L. J. Ricardi and L. Niro, "Design of a twelve-horn monopulse feed," *IRE Int. Conv. Rec., part. 1*, March 1961, pp. 49–56.
40. P. W. Hannan and P. A. Loth, "A monopulse antenna having independent optimization of the sum and difference modes," *IRE Int. Conv. Rec., part. 1*, March 1961, pp. 57–60.

41. B. Saka and E. Yazgan, "Pattern optimization of a reflector antenna with planar-array feeds and cluster feeds," *IEEE Trans. Antennas Propagat*., vol. 45, no. 1, January 1997.
42. R. F. Harrington, *Time Harmonic Electromagnetic Fields*, New York: McGraw-Hill, pp. 106–116, 1961.
43. L. Diaz and T. Milligan, *Antenna Engineering Using Physical Optics: Practical CAD Techniques and Software*, Boston: Artech House, 1996, pp. 193–196.
44. C. A. Balanis, "Green's functions" in *Advanced Engineering Electromagnetics*, Chapter 14, New York: John Wiley and Sons, 1989.
45. P. H. Pathak, "High frequency techniques for antenna analysis," *Proc. of the IEEE*, vol. 80, no. 1, January 1982.
46. Y. T. Lo and S. W. Lee (eds.), *Antenna Handbook: Theory, Applications and Design, Techniques for High Frequency Problems*, Chapter 4, New York: Van Nostrand Reinhold Co. Inc., 1988.
47. G. F. Paynter, T. H. Lee, and W. D. Burnside, "Expansion of existing EM Workbench for multiple computational electromagnetics codes," *IEEE Antennas and Propagation Magazine*, vol. 45, no. 3, June 2003.
48. D. Brunkow, V. N. Bringi, P. C. Kennedy, S. A. Rutledge, V. Chandrasekar, E. A. Mueller, and R. K. Bowie, "A description of the CSU-CHILL National Radar Facility,". *J. Atmos. Ocean. Tech*., 17, pp. 1596–1608, 2000.
49. M. Thomson, "The astromesh deployable reflector," *IEEE Symp. Antennas and Propag*., pp. 1516–1519, 1999.
50. M. Thomson, "Astromesh Deployable Reflectors for Ku and Ka-Band Satellites," *AIAA Symp*., 2002, pp. 1–4.
51. J. K. H. Lin, H. Fang, E. Im, and U. O. Quijano, "Concept study of a 35m spherical reflector system for NEXRAD in space application," presented at 47th AIAA/ASME/ASCE/AHS/ASC Structures, Structural Dynamics, and Materials Conference, Newport, RI, May 1–4, 2006.
52. R. Fowell and Wang, H., "Precision pointing of the Thuraya satellite." presented at 26th AAS Guidance and Control Conference, Breckenridge, CO, February 5–9, 2003.
53. R. C. Hansen, *Microwave Scanning Antennas*, New York Academic Press, New York, 1966; Los Altos, CA: Peninsula Publishing, 1985.
54. J. D. Walton, Jr. (ed.): *Radome Engineering Handbook*, New York: Marcel Dekker, 1970.
55. M. Skolnik (ed.): *Radar Handbook*, 2nd Ed., New York: McGraw-Hill, 1990.
56. M. Skolnik (ed.): *Radar Handbook*, 1st Ed., New York: McGraw-Hill, 1970.